AGU ADVANCING EARTH AND SPACE SCIENCE

Water Resources Research

RESEARCH ARTICLE
10.1029/2021WR031665

Controls on Stream Water Age in a Saturation Overland Flow-Dominated Catchment

Dana A. Lapides[1,2], W. Jesse Hahm[1], Daniella M. Rempe[3], William E. Dietrich[4], and David N. Dralle[2]

[1]Department of Geography, Simon Fraser University, Burnaby, BC, Canada, [2]Pacific Southwest Research Station, United States Forest Service, Albany, CA, USA, [3]University of Texas, Austin, TX, USA, [4]University of California, Berkeley, Berkeley, CA, USA

Key Points:

- Field observations of surface runoff, groundwater levels, and saturated extents indicate that saturation overland flow dominates streamflow
- Stable isotope tracers show that stream water age decreases as streamflow increases
- Streamflow is nevertheless mainly water greater than 1 day old, meaning that even overland flow is mostly not event water

Supporting Information:

Supporting Information may be found in the online version of this article.

Correspondence to:

D. A. Lapides,
danalapides@gmail.com

Citation:

Lapides, D. A., Hahm, W. J., Rempe, D. M., Dietrich, W. E., & Dralle, D. N. (2022). Controls on stream water age in a saturation overland flow-dominated catchment. *Water Resources Research*, *58*, e2021WR031665. https://doi.org/10.1029/2021WR031665

Received 24 NOV 2021
Accepted 25 MAR 2022

Author Contributions:

Conceptualization: Dana A. Lapides, W. Jesse Hahm, Daniella M. Rempe, David N. Dralle
Data curation: Dana A. Lapides, W. Jesse Hahm, David N. Dralle
Formal analysis: Dana A. Lapides, W. Jesse Hahm, David N. Dralle
Funding acquisition: W. Jesse Hahm, William E. Dietrich, David N. Dralle
Investigation: Dana A. Lapides, W. Jesse Hahm, William E. Dietrich, David N. Dralle
Methodology: Dana A. Lapides, W. Jesse Hahm, William E. Dietrich, David N. Dralle
Project Administration: David N. Dralle
Resources: W. Jesse Hahm, Daniella M. Rempe, David N. Dralle
Software: Dana A. Lapides, W. Jesse Hahm, David N. Dralle

Abstract Water age and flow pathways should be related; however, it is still generally unclear how integrated catchment runoff generation mechanisms result in streamflow age distributions at the outlet. Here, we combine field observations of runoff generation at the Dry Creek catchment with StorAge Selection (SAS) age models to explore the relationship between stream water age and runoff pathways. Dry Creek is a 3.5 km^2 catchment in the Northern California Coast Ranges with a Mediterranean climate, and, despite an average rainfall of ≈1,800 mm/yr, is an oak savannah due to the limited hillslope water storage capacity. Runoff lag to peak—after initial seasonal wet-up—is rapid (~1–2 hr), and total annual streamflow consists predominantly of saturation overland flow, based on field mapping of saturated extents and an inferred runoff threshold for the expansion of saturation extent beyond the geomorphic channel. SAS modeling based on daily isotope sampling reveals that streamflow is typically older than 1 day. Since streamflow primarily consists of overland flow, a significant portion of overland flow must not be event-rain but instead derive from older, nonevent groundwater returning to the surface, consistent with field observations of exfiltrating head gradients, return flow through macropores, and extensive saturation days after storm events. We conclude that even in a watershed fed primarily by overland flow, runoff is primarily not composed of event water. Our findings have implications for the interpretation of stream chemistry and the assumptions built into widely used hydrograph separation inferences, namely, the assumption that overland flow consists of new (event) water.

Plain Language Summary Streams that respond most rapidly to rainfall tend to be fed by a process called overland flow. This study uses high-frequency water tracking measurements to show that even in a watershed fed by overland flow, the water entering the stream during storm events tends to be older than the storm event causing the stream response. Hydrologic observations made during storm events reveal that water travels through the subsurface before reemerging as surface flow. The interaction between storm event water and subsurface soils and weathered bedrock likely lead to mixing such that the water entering the stream contains a substantial fraction of water from previous storm events.

1. Introduction

Do distinct runoff pathways give rise to particular stream water age distributions? Younger streamflow should derive from shorter or faster pathways such as overland flow, whereas older streamflow should derive from longer or slower pathways such as subsurface flow. Streamflow volumes can closely match precipitation input volumes over short timescales (hours-days), but there is widespread evidence—based on early isotopic evidence (e.g., Buttle, 1994; Neal & Rosier, 1990; Sklash, 1990) and more recent two-component hydrograph separation approaches (e.g., Freyberg et al., 2018), and fractal (e.g., Godsey et al., 2010; Kirchner et al., 2000) and StorAge Selection (SAS; e.g., Benettin et al., 2017; Rodriguez & Klaus, 2019; Visser et al., 2019) modeling studies—that stormflow typically consists of nonevent, older water (sometimes years old) displaced by or driven out of subsurface storage by new water (e.g., Hewlett & Hibbert, 1967).

One way to produce young stream water is for rain to reach the stream by flowing over the ground surface as overland flow (Elsenbeer et al., 1994; Elsenbeer & Lack, 1996; Shanley et al., 2002). SOF occurs when the water table rises from below and intersects the ground surface; the overland component of flow derives both from exfiltrating groundwater (return flow) and direct precipitation on saturated areas (DPSA; Dingman, 2015; Dunne & Black, 1970a, 1970b; Eshleman et al., 1993). Because the water table is dynamic, the area contributing to SOF

Supervision: W. Jesse Hahm, David N. Dralle
Visualization: Dana A. Lapides, W. Jesse Hahm, David N. Dralle
Writing – original draft: Dana A. Lapides, W. Jesse Hahm, Daniella M. Rempe, David N. Dralle
Writing – review & editing: Dana A. Lapides, W. Jesse Hahm, Daniella M. Rempe, William E. Dietrich, David N. Dralle

can vary over time, which has been referred to as the "variable source area" concept (Dunne & Black, 1970b; Wilson & Dietrich, 1987). SOF commonly occurs within convergent zones above channel heads (Dunne, 1978; Dunne & Black, 1970b; Kidron, 2021) and at the riparian-hillslope interface due to a rapid conversion of the tension saturated zone to atmospheric pressure with a small amount of added moisture from infiltration (Abdul & Gillham, 1984). SOF has also been documented to occur where small-scale heterogeneities in bedrock properties result in local exfiltrating head gradients (Wilson & Dietrich, 1987). In essence, SOF routes flow over the land surface when the subsurface flow capacity is overwhelmed; this interpretation is commonly reflected in hydrological models, where all water in excess of a shallow subsurface flow capacity threshold is routed to surface flow (e.g., Beven & Kirkby, 1979; Litwin et al., 2020). Thus, the age of SOF water should reflect the dominant source of that runoff, either from the subsurface via return flow (consisting of a mixture of relatively old, pre-event water and event water that has infiltrated) or direct precipitation on saturated areas (DPSA, consisting exclusively of newly arriving event water) that never infiltrates.

The relationship between hillslope runoff generation and the integrated age distribution at the catchment outlet is still largely opaque because few studies have evaluated travel time distribution models in places where runoff generation mechanisms have been directly documented (Benettin et al., 2017; Hrachowitz et al., 2021; Putnam et al., 2018; Rodriguez et al., 2018; Van der Velde et al., 2010; Wilusz et al., 2020). Resolving the impact of runoff generation mechanisms on age distributions would help to address the issue of equifinality in transit time distribution modeling and aid in the interpretation of the controls on stream geochemistry (Li et al., 2020; Torres & Baronas, 2021). Recently, Wilusz et al. (2020) used particle tracking to assess the relationship between runoff generation and transit times, while Rodriguez et al. (2018) compared modeled transit times using a conceptual model of catchment hydrology to empirically calculated transit times with good agreement. Benettin et al. (2017) found that little streamflow throughout the year was younger than 10 days at the Bruntland Burns site in Scotland, where saturation overland flow occurs on relatively flat peat-covered areas. Putnam et al. (2018) found that quickflow—which was primarily generated by SOF—was older than event water (i.e., water that derives from the driving rainfall) at the Pond Branch Catchment in Maryland. Sklash and Farvolden (1979) found that specific conductance and isotopic composition of overland flow water at the Hillman Creek watershed in Ontario, Canada, implied a strong contribution from groundwater. These findings suggest that SOF can be made up primarily of return flow, but controls on the relative fraction of pre-event and event water in SOF remain poorly understood.

Water transit time distributions (TTDs) describe the distribution of water ages in fluxes exiting a catchment control volume (e.g., Haggerty et al., 2002; Małoszewski & Zuber, 1982; Rodhe et al., 1996). Recently, StorAge Selection (SAS) functions have emerged as a tool for estimating TTDs directly from tracer data with minimal prior assumptions (Botter et al., 2011; Harman, 2015; Van Der Velde et al., 2012). SAS functions define what fraction of outflows (e.g., evapotranspiration and streamflow) derive from different water ages in storage. The SAS function framework is grounded in a catchment mass balance; the integrated collection of water ages in storage gives rise to an observed tracer time series in effluxes via preferential "selection" of different storage ages. Studies have found that SAS functions vary through time as a function of catchment state (e.g., Benettin et al., 2017; Harman, 2015; Kim et al., 2016), and that the water storage tends to drain younger water to streamflow when the catchment is wetter (referred to in literature as the inverse storage effect, e.g., Benettin et al., 2017; Harman, 2015).

Here, we combine field observations at the intensively monitored Dry Creek catchment in Northern California with water age modeling using SAS functions to evaluate how SOF mechanisms impact water ages in streamflow. We interpret catchment-integrated isotopic signals in streamflow with intensive field observations of water storage dynamics, runoff generation, saturated extent, groundwater levels, and head gradients. Specifically, we address the following questions:

1. How old is streamflow in a saturation overland flow-dominated catchment?
2. How does the portion of event water in streamflow change as the dominant runoff generation mechanism shifts through storm events?
3. Using transit time models and field observations of runoff generation, what portion of saturation overland flow comes from return flow versus direct precipitation on saturated areas (DPSA)?

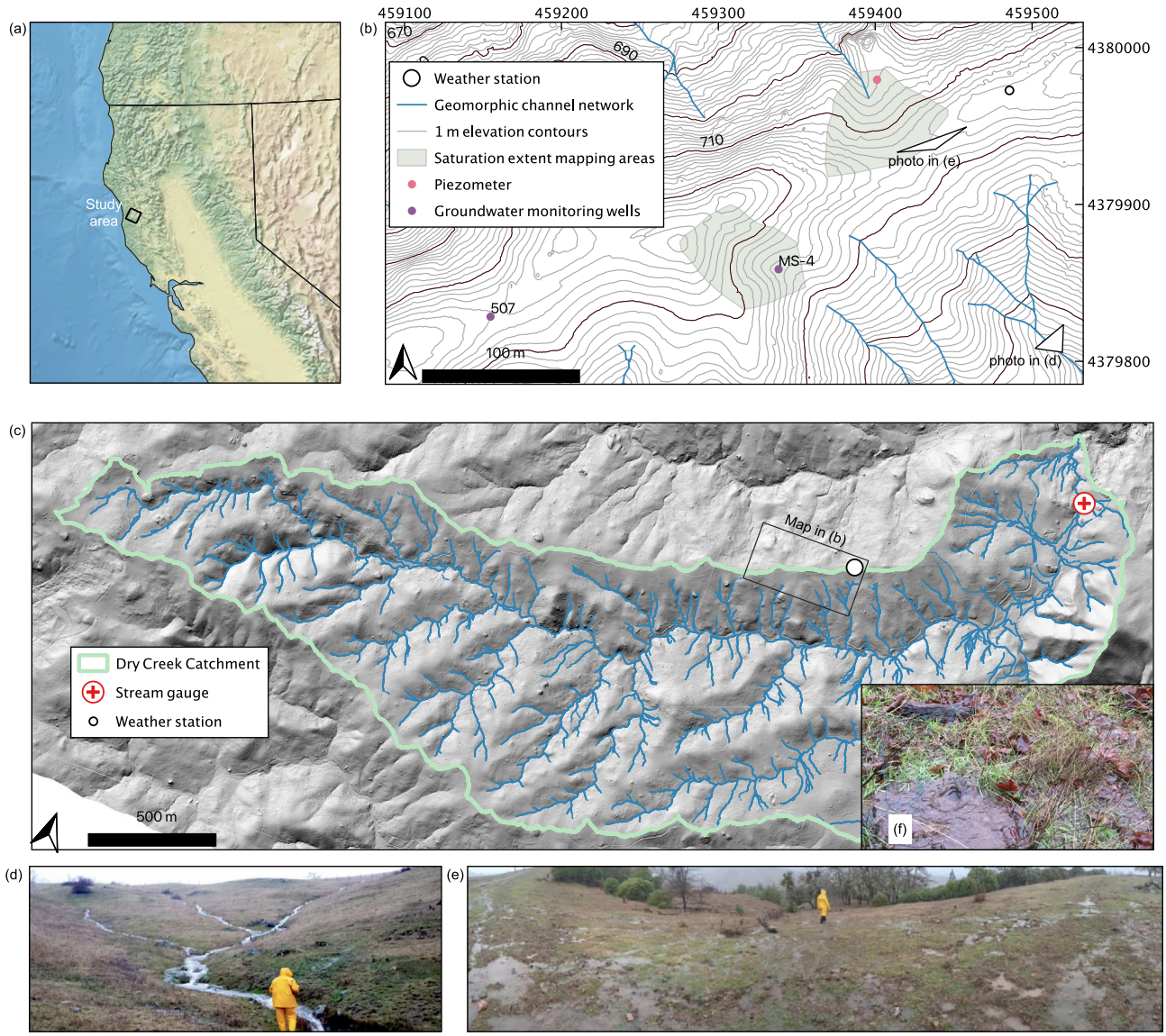

Figure 1. (a) Location map of study site in the Northern California Coast Ranges, on Natural Earth hillshade layer. (b) Map showing study ridge, with lidar-derived 1-m (thin lines) and 10-m (bold lines) elevation contours. (c) Map showing Dry Creek catchment, on lidar-derived hillshade. Blue lines mark the streamflow network calculated from the 1-m DEM. (d) Photo of flowing gully network during storm event. (e) Panoramic photo of study ridge during storm event showing saturation. (f) Visible return flow through a macropore.

2. Methods

2.1. Study Site

The study catchment, Dry Creek (3.5 km^2; outlet at 39.5754°, −123.4642°) is in the Eel River watershed, in the Northern California Coast Ranges (Figure 1a) about 200 km north of San Francisco, in the traditional territory of the Coast Yuki, the California Dene (Athabaskan), and Pomo (Baumhoff & Merriam, 1958; Foster, 1944; Johnson, 1979; Stewart, 1943). Dry Creek is within a ranch named Sagehorn, which has been part of the Eel River Critical Zone Observatory since 2015. The site experiences a Mediterranean climate, with a mean annual temperature of 13.3°C and mean annual precipitation of 1,800 mm (Group, 2013), almost all of which falls as rain between October and May.

The site is underlain by the Central belt mélange of the Franciscan complex (Jayko et al., 1989). The mélange bedrock is a sheared argillageous matrix with embedded blocks of diverse lithologies, including greywacke

(sandstone) and chert. Larger blocks of greywacke cover less than 15% of the site by surface exposure (Lovill et al., 2018). The primary mineralogy of the mélange matrix is quartz, microcline, albite, muscovite, chlorite, illite, titanite, minor gypsum, pumpellyite and lawsonite, and rare kaolinite and carbonate (Cloos, 1983; Hahm, Rempe, et al., 2019).

Soils developed on the mélange matrix are mollisols (Hahm, Rempe, et al., 2019; Rittiman & Thorson, 2001). More than 50 pits and augered holes indicate that the soils are typically 50 cm thick (ranging from 30 to 70 cm), with an upper organic-rich O horizon and a lower clay-rich Bt horizon. Guelph permeameter measurements of saturated hydraulic conductivity document high conductivities in the near surface that are similar to the maximum recorded rainfall intensities (Dralle et al., 2018). Pervasive animal burrowing and plant rooting has resulted in abundant macroporosity in the upper portion of the soil.

Deep drilling across the site (locations denoted with groundwater monitoring wells mapped in Figure 1b, all well locations shown in: Hahm, Rempe, et al., 2019) revealed that the in situ mélange beneath the soils is seasonally unsaturated and weathered to depths of 2–4 m (Hahm, Rempe, et al., 2019), with abundant yellow-red oxidation. Below this depth, the parent material is permanently saturated, blue-black in hue, and has extremely low hydraulic conductivity. Dry Creek drains to the east through a hilly landscape (mean gradient of 28%) typical of the Central belt mélange. A dense gully network is incised into inactive, deep-seated earthflows that have given the site a "melted ice-cream" appearance (Kelsey, 1978). Grazing by sheep (historically) and cattle (contemporary) has been relatively light, and no terracettes have formed. The geomorphic channel drainage network (defined by channels with banks and clear elevation contour indentations visible on bare-earth lidar-derived maps) is shown in Figure 1c, and has a relatively high density of 16.9 km/km^2, with an average upslope contributing area of 1,085 m^2 at channel heads (Lovill et al., 2018). Hillslopes are convex-up, with typical divide-to-channel horizontal distances of 10–20 m (Figure 1). Dry Creek's catchment-averaged denudation rate, inferred from cosmogenic nuclides in quartz stream sediment, is 0.12 mm/yr (Hahm, Rempe, et al., 2019). The region has been uplifting and eroding for the past 3 Ma, with the emergence of the Northern California Coast Ranges from sea level accompanying the northward migration of the Mendocino Triple Junction (Atwater & Stock, 1998; Lock et al., 2006).

Despite high mean annual precipitation, the plant community developed on the mélange matrix is an oak savanna (Hahm et al., 2017, 2018), with primarily European annual herbaceous groundcover that senesces in the summer dry season and a patchy, sparse overstory of winter-deciduous Oregon White Oak (*Quercus garryana*).

2.2. Description of Hydrologic Field Monitoring Infrastructure

The National Center for Airborne Laser Mapping (NCALM) flew lidar at the site in 2015; a 1 m pixel sized elevation DEM was used to generate the maps in Figure 1. A weather station on the ridgetop records precipitation with a Campbell Scientific TB4 tipping bucket gauge, and is corrected for wind-induced undercatch, as described in Hahm, Rempe, et al. (2019). Stream stage is recorded at the outlet with a Solinst Levelogger pressure transducer, with local atmospheric correction. Stream gauging methods are described in Hahm, Rempe, et al. (2019).

This study capitalizes on the substantial existing monitoring network at Dry Creek to explore SOF (Hahm et al., 2020; Hahm, Rempe, et al., 2019). Nine groundwater monitoring wells were completed with continuously slotted PVC-wells and outfitted with Solinst Levelogger and Campbell Scientific CS451 pressure transducers to continuously monitor water table fluctuations; 2 years of groundwater levels for all wells are shown in Hahm, Rempe, et al. (2019), and in this study data from two representative wells are used (MS4 and 507). We installed a 2.54 cm solid PVC piezometer (MNP3) via hand auger to a depth of 55 cm in a side-slope about 5 m horizontally above a channel head. The lowest 5 cm was slotted and screened, back-filled with sand, and sealed with bentonite. A Solinst pressure transducer was used to monitor head, with 20 cm of casing stick-up above the ground surface to capture possible artesian conditions. Drilling observations revealed that the piezometer opening was below the Bt horizon (which was encountered at 35 cm depth), and within typical smeary, gray-yellow, clay-rich mélange matrix weathered bedrock.

2.3. Precipitation and Stream Water Stable Isotopic Composition

2.3.1. Collection

We measured the stable isotopic composition of hydrogen in both precipitation and stream water as a tracer for interpreting travel times. The isotope sampling program and analysis methods were first described in Hahm et al. (2020) in a study of oak water sourcing dynamics. Starting 10 December 2015 through the end of the 2020 water year, precipitation samples were collected daily when sufficient precipitation had fallen, typically between 06:00 and 08:00, approximately 1.3 km west of the weather station in an open field at an elevation of 645 m a.s.l, and stored in 30 mL HDPE bottles until analysis. When snow fell (which was rare), it was allowed to melt into the sample collector before sampling. Stream water samples were collected from near the mouth of Dry Creek when water was present in the channel on a semiperiodic campaign basis that began in Fall 2015, followed by two complete years of daily sampling (typically between 8:00 and 9:00) during the 2018 and 2019 water years (sampling location = 39°34′22.57″N, 123°27′46.76″W; 3.5 km^2 drainage area). Groundwater samples were collected on a semiperiodic basis via bailer from two monitoring wells (MS4 and 507), from a depth ranging from the water table surface to 1 m below the water table surface.

2.3.2. Analysis

Following the same methodology as described in detail in Hahm et al. (2020), all samples were analyzed at the UC Berkeley Center for Stable Isotope Biogeochemistry via Isotope Ratio Mass Spectroscopy on a Thermo Delta PLUS XL instrument. Data are expressed in per mil delta notation (‰) relative to Vienna Standard Mean Ocean Water (VSMOW): $\delta D\ ‰ = \left(\frac{R_{sample}}{R_{standard}} - 1\right) 1,000$, where R is the ratio between the heavy and light isotope (i.e., D to H). The long-term precision is 0.60‰ δD (Hahm et al., 2020).

To ensure the completeness of the rainfall isotope time series, we compared rainfall time series from the ridge-top weather station (Figure 1) with the set of timestamps on which precipitation was sampled. We identified all time intervals during the study period for which more than 5 mm of rain fell but no sample collection was recorded in the following 48 hr. These criteria were chosen so that rain events reasonably small enough to evaporate and/or transpire completely would not be detected and so that a rain event sampled the next day would not be recorded as missing. We identified 25 dates with missing data (compared to the existing record of 348 samples). Six of the missing samples were likely misplaced prior to sample analysis, and the remaining 19 were not sampled. When samples were not collected, any rainfall would mix with samples in the following days until the next sample was collected; thus, the next sample collected would represent the average concentration in rainfall over the intervening rainfall events. We replaced missing dates for which no sample was taken with the next measured isotope value if the next sample was taken within 3 days (1 date).

To fill the remaining missing dates, we performed a linear regression between rainfall isotope concentrations at Sagehorn and the nearby Angelo Coast Range Reserve ("Angelo," 23 km northeast; sampling program is described in Oshun et al., 2016). For all dates with missing Sagehorn rainfall isotope samples, we identified an Angelo rainfall sample as close in time to the missing sample as possible (no more than 2 days later) and used the linear relationship between Sagehorn and Angelo rainfall isotope data to fill in an appropriate value for the missing Sagehorn data. Only 10 dates remained with missing data after this process, representing a negligible fraction of precipitation input during the study period.

2.4. Event Runoff Analysis

2.4.1. Lag to Peak

We quantified the lag from rainfall centroid to peak streamflow response for all storm events with well-defined beginnings and ends (manually identified) for both Dry Creek and for the topographically and geologically similar Hank Creek that neighbors Dry Creek to the north (see Lovill et al., 2018 for a map). Hank Creek has a 56% larger catchment area at the gauging location (see maps in Lovill et al., 2018). The streamflow sensor sampling frequency is 15 min, which represents the precision of the analysis.

2.4.2. Runoff Ratio

Graphical hydrograph separation following the method of Hewlett and Hibbert (1967) was performed for 47 Dry Creek storm events spanning the 2016–2019 water years, to quantify how the amount of "quickflow" generated

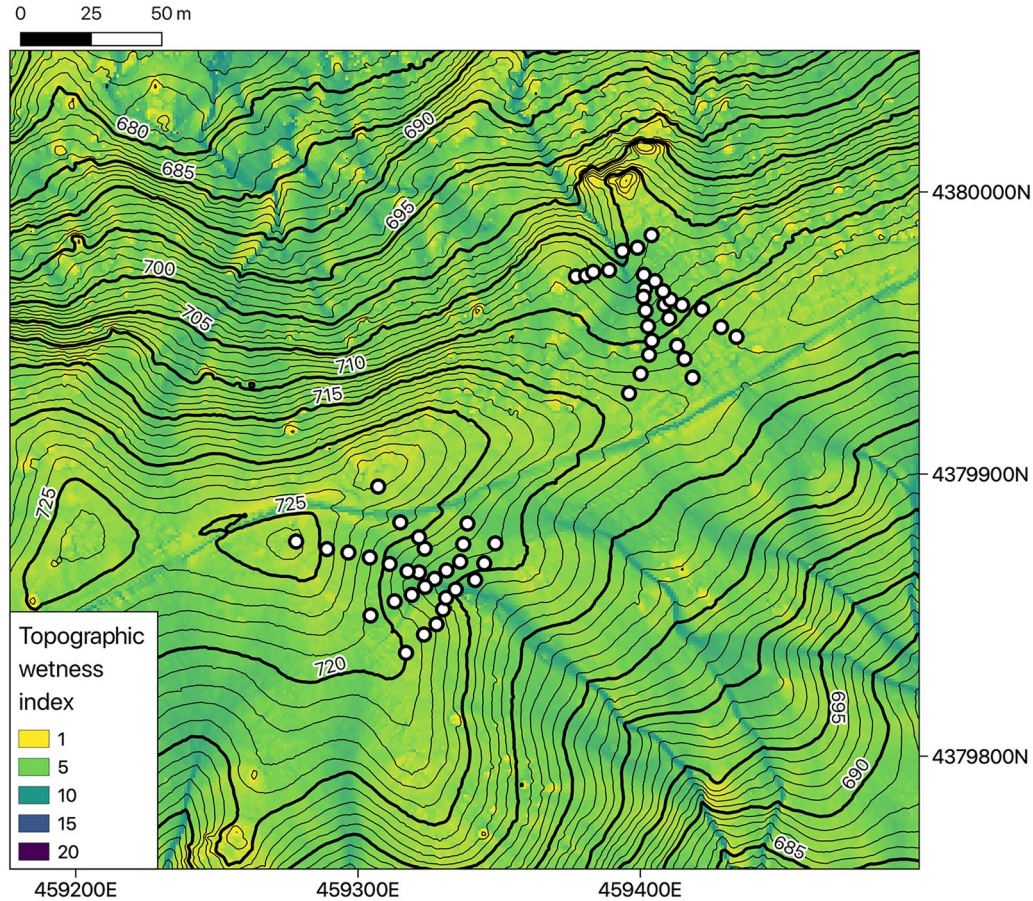

Figure 2. One-meter contour map of the ridge where surface saturation observations were performed. Background colors indicate topographic wetness index, and white circles mark the locations of saturation observation pits. See Equation 1 for the definition of topographic wetness index.

(the streamflow generated in excess of pre-event "baseflow") varies in relation to pre-event catchment storage state (quantified by the streamflow magnitude at the start of the event) and storm event size. Events were chosen in such a way that the hydrograph recession was not interrupted by a new rainfall event. As Latron et al. (2008) note, this hydrograph separation approach is arbitrary, and the water volumes separated are not interpreted in terms of runoff pathway origin or age via this method. Although more sophisticated hydrograph separation methods are available (e.g., Blume et al., 2007), the graphical approach is simple, has seen widespread and sustained use, and is presented here as a diagnostic that informs catchment rainfall response, similar to the lag-to-peak analysis. Here we also report the event runoff ratio (quickflow as a fraction of event precipitation).

2.5. Surface Saturation—Observations and Model

Over the course of a multiday storm event in January 2018, surface saturation extents were mapped in two zero-order catchments straddling the northern ridge of Dry Creek (Figure 1). A total of 57 shallow saturation observation pits (see Figure 2) were dug to a depth of approximately 2 cm below the soil surface, and marked with flags to facilitate locating. At seven different times corresponding to a range of different flow values in the stream, the pits were logged as either saturated or not saturated, depending on whether or not a free water surface was observed in the pits, similar to the qualitative wetness classification presented in Rinderer et al. (2012). It was assumed that the presence of a free water surface indicated that the shallow water table at the site had intersected the ground surface at that point, thus potentially contributing to saturation overland flow.

A multi-variate logistic regression was then formulated using the observed saturation data to predict saturation state at all points within the catchment as a function of log-transformed discharge at the catchment outlet, and a topographic wetness index (TWI), calculated as:

$$\mathrm{TWI} = \ln\left(\frac{a}{\tan\beta}\right) \tag{1}$$

where a [m] is contributing area per unit length contour (calculated using the r.flow module within GRASS GIS) and β was the topographic slope (Beven & Kirkby, 1979). Calculations were made on a 1 m resolution DEM derived from Dietrich (2015). Across the saturation observation pits, TWI ranges from 3.1 to 8.8, with a median of 5.0. Across the landscape, the 10th, 50th, and 90th percentile of TWI values are 3.1, 4.6, and 6.4, respectively. Within the logistic regression, streamflow encodes the time dependence so that saturated area expands and contracts with catchment wetness state, and TWI encodes topographic position on the landscape. More convergent areas are both more likely to be saturated for a given wetness state and have a higher TWI. Measures of topographic position and wetness state are the primary drivers of saturation on the landscape.

Using the logistic regression model for saturation, the stream discharge record, and a catchment-wide map of TWI, spatially explicit saturation extent maps were generated at all times throughout the period of flow record. At the catchment scale, saturation extent is reported as the percentage of points within the catchment classified as saturated at a given point in time. Note that at the catchment scale, saturated area is effectively a function of discharge in the stream since the spatial distribution of TWI in the catchment is constant. We then quantify direct precipitation on saturated areas by multiplying instantaneous rainfall intensities by saturated areas determined from instantaneous streamflow.

2.6. Estimating the Volume of Overland Flow

We conceptualize runoff generation at Dry Creek as a fill and spill process, as in McDonnell et al. (2021). During a storm, the water table rises to the ground surface, at which point the subsurface can no longer store additional water. When the subsurface is at full capacity, it transmits subsurface flow to the stream at a constant maximum rate (e.g., Beven & Kirkby, 1979; Litwin et al., 2020). If streamflow exceeds the maximum subsurface contribution, overland flow must account for the additional discharge. We motivate the selection of a subsurface flow capacity using field observations as well as results from our logistic regression model for saturation extent. Then, overland flow can be calculated by subtracting the constant flow threshold from the discharge time series, setting all negative values to 0. For a visual depiction of how overland flow was calculated, see Figure S11 in Supporting Information S1.

2.7. StorAge Selection (SAS) Functions

SAS functions describe quantitatively how waters of different ages are selected from an age-ranked storage distribution to constitute a catchment efflux (ET or streamflow) (Botter et al., 2011; Harman, 2015; Van Der Velde et al., 2012). The basic mass balance is given as:

$$\frac{\partial S_T(T,t)}{\partial t} + \frac{\partial S_T(T,t)}{\partial T} = J(t) - Q(t)\Omega_Q\left(S_T(T,t),t\right) - ET(t)\Omega_{ET}\left(S_T(T,t),t\right), \tag{2}$$

where t is time [T] and T is age [T]; $S_T(T, t)$ [L] is the system age-rank storage; $J(t)$ [L/T] is precipitation input, $Q(t)$ [L/T] is streamflow output, and $ET(t)$ [L/T] is evapotranspiration output; Ω_Q [$\cdot$] and Ω_{ET} [$\cdot$] are cumulative SAS functions for Q and ET, respectively, that determine the output age cumulative distribution function given the age-rank storage at each time. The corresponding SAS functions ω_Q and ω_{ET} are the derivatives with respect to T of Ω_Q and Ω_{ET}. A boundary condition of $S_T(T = 0, t) = 0$ is assumed, and an initial storage $S_T(T, t = 0)$ must be parameterized. Since initial age-rank storage is never known, a spin-up period is used to identify a reasonable catchment state to use as the initial condition.

A conservative tracer can be used to constrain water age distributions in streamflow and evapotranspiration through the following relation:

Table 1
Parameters Tuned in StorAge Selection Model Using Monte Carlo Simulation

Parameter	Definition
$kmin_Q$	Minimum exponent for Q SAS function as defined in Equation 6 [·]
$kmax_Q$	Maximum exponent for Q SAS function as defined in Equation 6 [·]
logfactor_Q	Scaling between $kmin_Q$ and $kmax_Q$ as defined in Equation 6
k_{ET}	ET SAS function power in Equation 4 [·]
S_0	Initial storage [mm]
C_{S_0}	Initial isotopic concentration in storage [δD‰]

$$C_Q(t) = \int_0^{S_{tot}} C_S(S_t, t)\omega_Q(S_T, t)dS_T. \tag{3}$$

where C_Q [·] is the concentration of tracer in streamflow, C_S [·] is the distribution of tracer concentration in age-ranked storage, and Ω_Q is the SAS function. An analogous equation to Equation 3 exists for ET as well. However, the role of ET in this study is minimal since ET is not constrained by flux measurements or concentrations and constitutes a significantly smaller flux than P or Q during the wet season on which this study is focused.

We followed the method described by Benettin and Bertuzzo (2018) to calculate the SAS function. Benettin and Bertuzzo (2018) provided a MATLAB implementation of the method, which we translated into the Python programming language (https://www.python.org/). An alternate Python implementation was developed by Harman et al. (2019). For a full description of the numerical methods used in this study, see Benettin and Bertuzzo (2018). The only difference is that in our implementation, we use a standard forward Euler numerical scheme, as opposed to the modified Euler method outlined by Benettin and Bertuzzo (2018). Although six options are available in our code, in this study we use a constant power law SAS function for ET:

$$\Omega_{ET} = \left(\frac{S_T(T,t)}{S(t)}\right)^{k_{ET}}, \tag{4}$$

where $S(t)$ is total storage and $k_{ET} \in (0, \infty)$ is a parameter. For the streamflow SAS function, we use a time-varying power law (Benettin et al., 2017):

$$\Omega_Q = \left(\frac{S_T(T,t)}{S(t)}\right)^{k_Q}, \tag{5}$$

where the parameter k_Q [·] varies between a minimum value $k_{\min_Q}$and a maximum value $k_{\max_Q}$with a log dependence on wetness state wi:

$$k_Q(t) = k_{\min_Q} + \left(k_{\max_Q} - k_{\min_Q}\right) \log\left[\left(1 - \text{logfactor}_Q\right) wi\right] \tag{6}$$

where wi is the log-transformed instantaneous stream runoff normalized to the maximum log-transformed stream runoff at the outlet, and logfactor_Q [·] is a constant parameter. A time-varying power law has been shown to capture system dynamics well (Benettin et al., 2017), and a log dependence rather than a linear dependence provides more flexibility in how the catchment transitions from a wet to a dry state due to the addition of an extra parameter. We used the time period of 1 October 2017 to 1 October 2018 as a representative spin-up period repeated 10 times to generate an initial condition for age-rank storage. Model calibration was performed using all data through the 2019 water year, with the top 95th percentile of parameter sets retained. Model evaluation was performed on the 2020 water year to evaluate performance of these parameter sets.

We determined best fit parameter sets by randomly sampling the parameter space (see Table 1 for a list of tuned parameters) via Monte Carlo simulation on 10,000 parameter sets. Parameter calibration was done using the set of collected data from 1 October 2016 to 1 October 2019. We evaluated model fit using the Nash-Sutcliffe model efficiency coefficient (NSE):

$$NSE = 1 - \frac{\Sigma_{t=1}^{t=t_0}\left(C_m^t - C_0^t\right)^2}{\Sigma_{t=1}^{t=t_0}\left(C_0^t - \bar{C}_0\right)^2}, \tag{7}$$

where time t ranges from the beginning ($t = 1$) to the end ($t = t_0$) of the model simulation, C_m^t is the modeled streamflow concentration at each time, C_0^t is the observed streamflow concentration at each time, and $\bar{C}_0$ is the mean of observed streamflow concentrations (Nash & Sutcliffe, 1970) and Kling-Gupta Efficiency (KGE):

$$KGE = 1 - \sqrt{(r-1)^2 + (\alpha - 1)^2 + (\beta - 1)^2}, \tag{8}$$

where r is the linear correlation coefficient between modeled and observed data, $\alpha = \sigma_m/\sigma_o$ is the ratio between modeled and observed standard deviation, and $\beta = \left(\bar{C}_m - \bar{C}_o\right)/\sigma_o$. NSE > 0 or KGE > −0.41 indicates that the model performs better than a model defined as the mean of the data for all time (Knoben et al., 2019). After parameterization, performance was evaluated on data from 1 October 2019 to 1 October 2020. Previous SAS modeling studies which found model performance to be adequate have found maximum NSE ranging from 0.24 to 0.92 (Benettin et al., 2017; Harman, 2015; Rodriguez et al., 2021; Rodriguez & Klaus, 2019; Smith et al., 2018; Van Der Velde et al., 2012), and Kirchner (2003) suggested that a successful behavioral model has NSE > 0.5 and KGE > 0.3. We rank model performance by the product of NSE and KGE, with successful behavioral performance above 0.15. Using the top 95th percentile of parameter sets, we calculated ensemble means with 25th–75th percentile and 10th–90th percentile uncertainty ranges for: modeled isotope concentration, median storage and streamflow ages, fraction of streamflow younger than 1 day old, and fraction of streamflow that derives from the youngest tenth percentile of storage.

2.7.1. Mass Balance Closure in SAS Model

Since evapotranspiration (ET) was estimated using the Hargreaves equation for potential ET rather than observed actual ET, the representation of evapotranspiration (ET) used to parameterize the SAS model likely does not fully capture the dynamics of ET in the Dry Creek catchment. This is visible from examining the long-term, increasing trend in catchment storage. To correct for this, we adjusted ET based on a running mass balance:

$$\frac{d}{dt}S = P - ET - Q \tag{9}$$

where S [L/T] is dynamic catchment storage. Over long time periods, we assume changes in storage are negligible at Dry Creek; small water storage capacity and large average P result in repeated annual storage dynamics and minimal interannual hydrological memory (Dralle et al., 2018; Hahm, Dralle, et al., 2019; Hahm, Rempe, et al., 2019). We therefore adjust ET by subtracting the linear trend fit to storage on 1 October of each year, resulting in no systematic increase in storage over time. The choice to linearly detrend storage, rather than to subtract a storage state-specific value, should have a minimal impact on SAS modeling results since ET is much smaller than Q during the wet season.

2.7.2. Limitations of a Daily Sampling Interval

The highest frequency of regular sampling in our isotope data is daily, raising the question of whether a daily sampling interval is adequate to constrain water ages at shorter timescales, despite a constant model timestep of 4 hr. Rodriguez and Klaus (2019) found that a composite SAS function was required to represent isotope dynamics on shorter timescales, a finding that suggests that a higher sampling rate could reveal inadequacies in the functional form of the SAS function used here that do not appear in our study, which includes no subdaily sampling. Such inadequacies could impact results about the fraction of water younger than 1 day. To address this concern, we performed a synthetic experiment. Using a synthetic time series of stream isotope data with a high fraction of water younger than 1 day, we explored the impact of coarsening sampling frequency (unit, 2×, 4×, 8×, 16×) on model calibration results (Text S4 in Supporting Information S1). We found that decreasing the sampling frequency from 1 to two or 4 days (coarsening by 2× or 4×) had a negligible impact on the estimated fraction of water younger than 1 day (unit frequency), indicating that the fraction of water younger than a unit frequency is fairly robust to coarsening in sampling frequency. Thus, a sampling interval of 1 day should be adequate to have confidence in fraction of water younger than 1 day.

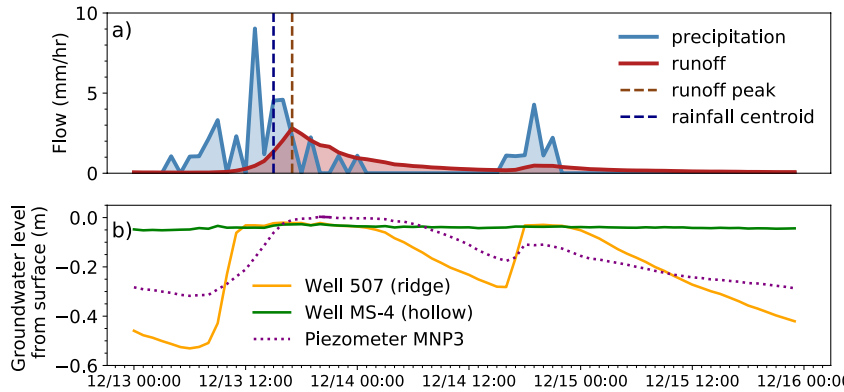

Figure 3. Hydrologic response at Dry Creek in response to a representative wet-season storms on 12–15 December 2018 with a runoff coefficient of 0.54 for the first event. (a) Streamflow is sampled at 15 min intervals and precipitation is sampled at 5 min intervals. Both are smoothed to hourly resolution. Lag to peak is 2 hr for the first event. (b) Concurrent groundwater response measured at two wells and one piezometer. Solid line in piezometer data indicates artesian head condition.

3. Results

3.1. Catchment Hydrologic Response to Winter Storms

3.1.1. Hydrograph Features and Runoff Sources

At the end of the summer dry season, shallow and deep unsaturated soil moisture stores and weathered rock moisture are depleted at Dry Creek (Hahm et al., 2020). The first rains increase moisture content in the unsaturated zone without causing a groundwater response (Dralle et al., 2018). Groundwater responds after approximately 100 mm of cumulative rainfall, and about 200 mm is sufficient to raise water tables to or near the ground surface (Dralle et al., 2018). Storage then depletes at the start of the dry season, and, as its name implies, Dry Creek typically ceases to flow by late May or early June (Dralle et al., 2018; Lovill et al., 2018).

During storm events (example in Figure 3a), large volumes of water commonly exfiltrate via macropore flow (see Figure 4a) and return flow, and artesian conditions and vertical head gradients are observed in piezometers (solid line in piezometer data in Figure 3b). Periods of time with artesian head conditions represent a lower bound estimate of the times during which exfiltrating head gradients exist in the catchment. Winter runoff in Dry Creek is dominantly sourced from saturation overland flow (in the sense of Dunne and Black (1970b) and Dunne (1978)) and shallow subsurface flow in the weathered portion (upper few meters) of the subsurface, as illustrated schematically in Figure 4b (Dralle et al., 2018). The subsurface critical zone at Dry Creek consists of a 2–4 m thick layer of organic soils and clay-rich weathered bedrock matrix overlying unweathered, perennially saturated mélange, as shown in Figure 4a (Hahm, Rempe, et al., 2019). The shallow depth to fresh bedrock results in relatively small integrated porosity and water storage capacity, causing widespread saturation overland flow during the winter wet season.

Lag to peak and event runoff coefficients also support widespread SOF. Across analyzed storms, Dry Creek's lag to peak time was on average 2.5 ± 1.6 hr (±1 s.d.), and neighboring Hank Creek's was 3.0 ± 1.5 hr, as shown in Figure 5a. These times are typical for catchments of comparable area experiencing saturation overland flow according to the commonly depicted timescales in Dingman (2015)'s *Physical Hydrology* textbook (after Kirkby (1988), based on data from Dunne (1978)). The event-based runoff ratio at Dry Creek is variable and spans the full range from 0 to 1 (Figures 5b and 5c). The runoff ratio is uncorrelated with the catchment storage state (wetness) at the start of a storm event, quantified via the streamflow just before the initial stream response (Figure 5b). In contrast, the total precipitation in the event explained 39% of the variance in runoff ratio, with events smaller than 25 mm generally producing runoff ratios less than 0.5, and events greater than 25 mm producing runoff ratios greater than 0.5 (Figure 5c).

3.1.2. Surface Saturation in Response to Storms

Saturation extent measured via discrete mapping campaigns correlated with discharge at the catchment outlet (Figure 6); as discharge decreased in both zero-order catchments (a–f and g–l), the number of saturation obser-

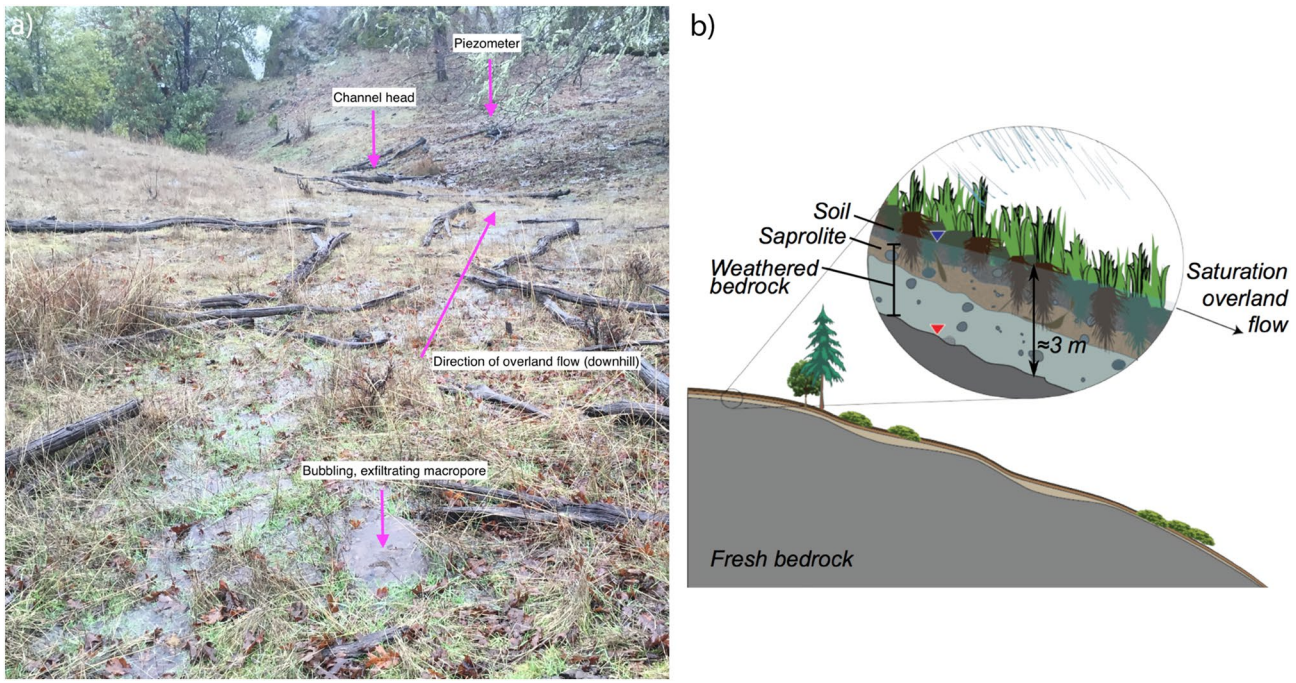

Figure 4. (a) Photo illustrating widespread saturation overland flow, an exfiltrating macropore, and the location of the piezometer on a hillslope above a channel head during a break in the rain on 17 January 2016 at 13:20, when the runoff in Dry Creek was 125 mm/day. (b) Conceptual cross section of the critical zone in the Dry Creek watershed, showing relatively thin weathered zone (~3 m), location of extreme end-member summer (red) and winter (blue) water table locations via inverted triangles, and runoff generation mechanisms. Modified from Hahm, Rempe, et al. (2019).

vation pits at both catchments decreased as well. These mapping campaigns spanned nearly the full range of discharge throughout the study period (Figure 7a), and the observation locations' TWI range closely matches that of the catchment at large. The logistic regression model shown in Figure 7a used to predict saturation as a function of catchment discharge and topographic wetness index (TWI) has an accuracy of 83% on observed data.

By applying the logistic regression model, we found that the dynamic extent of saturated area grows throughout a storm event and shrinks as the water table recedes from the surface (Figure 7b; Video S1), with portions of the

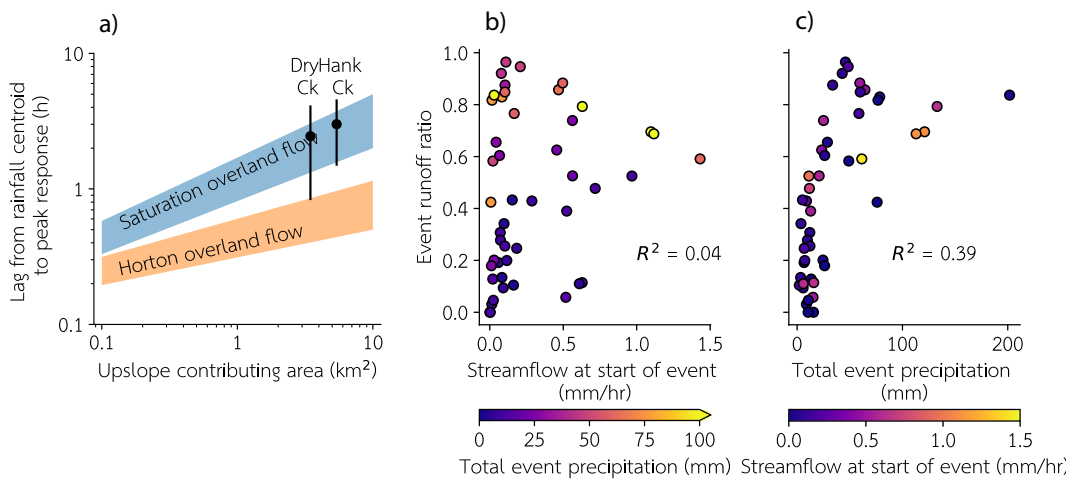

Figure 5. (a) Peak streamflow lag times from rain event centroids (mean ±1 s.d.) as a function of drainage area, plotted on regions typical of two overland flow generation mechanisms. Shaded areas and plotting space from Dingman (2015), after Kirkby (1988), based on data from Dunne (1978). (b, c) Event-based runoff ratios at Dry Creek as a function of pre-event streamflow (b) and total event rainfall (c).

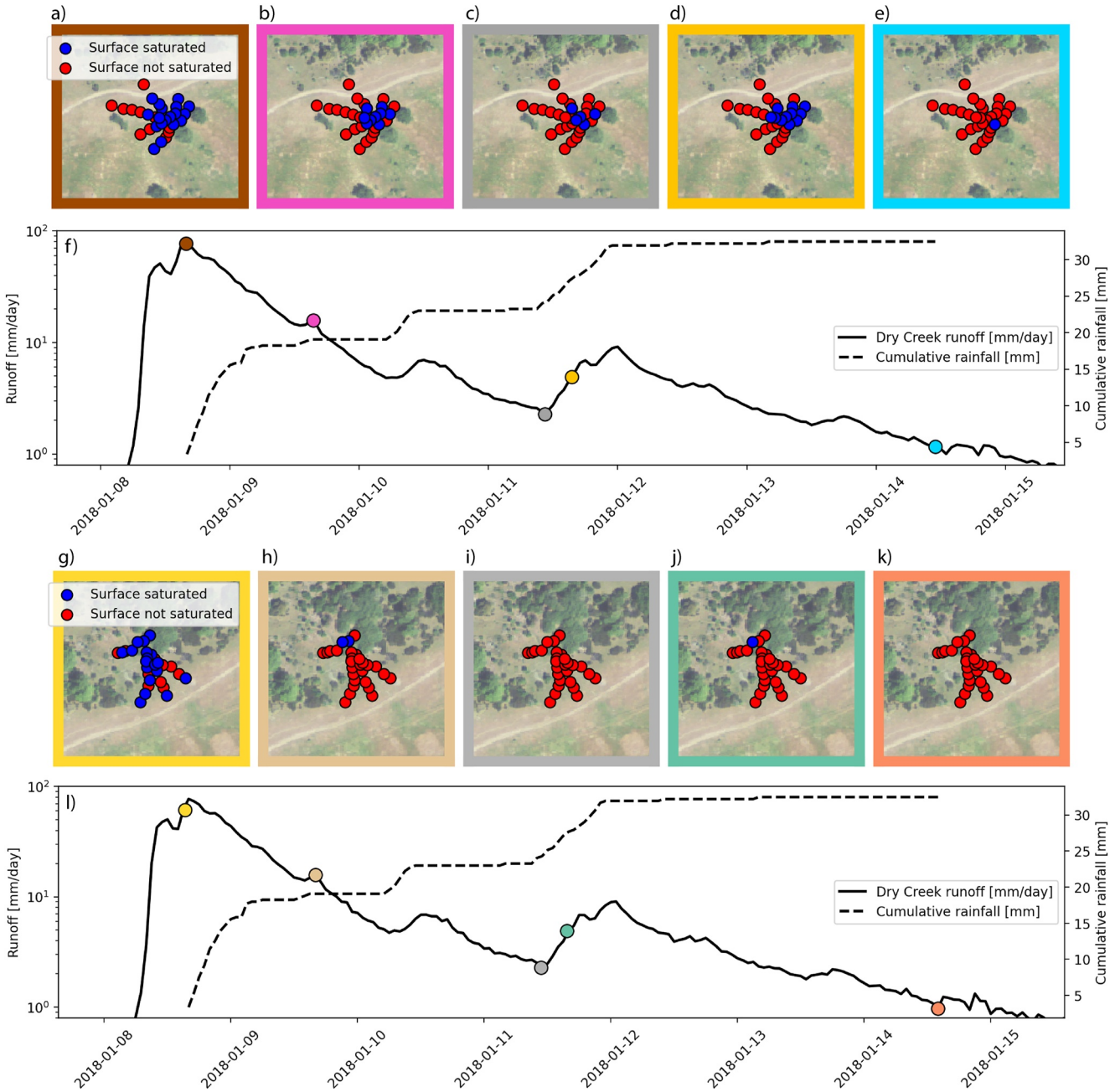

Figure 6. Observations of surface saturation during a streamflow recession in January 2018 at two zero-order catchments located in (top) Dry Creek and (bottom) Hank Creek, bordering Dry Creek. For a map contextualizing the location of the saturation observation pits, see Figure 2. Panels (a–e) and (g–k) show mapped saturation extent during each field visit. Border colors for each panel correspond to the dots with the same color in panel f (a–e) or l (g–k).

surface of the catchment remaining saturated and contributing to overland flow for days following a precipitation event. At runoff rates with the highest relative runoff contribution, the logistic regression model suggests that more than half of the catchment is saturated (Figure 7a). An instantaneous runoff rate of 2 mm/day at the catchment outlet (not shown) was the threshold above which saturation extends beyond the stream channel, according to the logistic regression model. At runoffs of 10 mm/day, saturation is widespread outside of the channel (Figure 7b). Based on these results, as well as field observations of overland flow corresponding to comparable catchment discharge states, we chose 5 mm/day (best estimate; likely range between 2 and 10 mm/day) as a threshold runoff rate that corresponds with the maximum subsurface flow capacity adjacent to the channel network, such that the streamflow rate above 5 mm/day derives mostly from saturation overland flow.

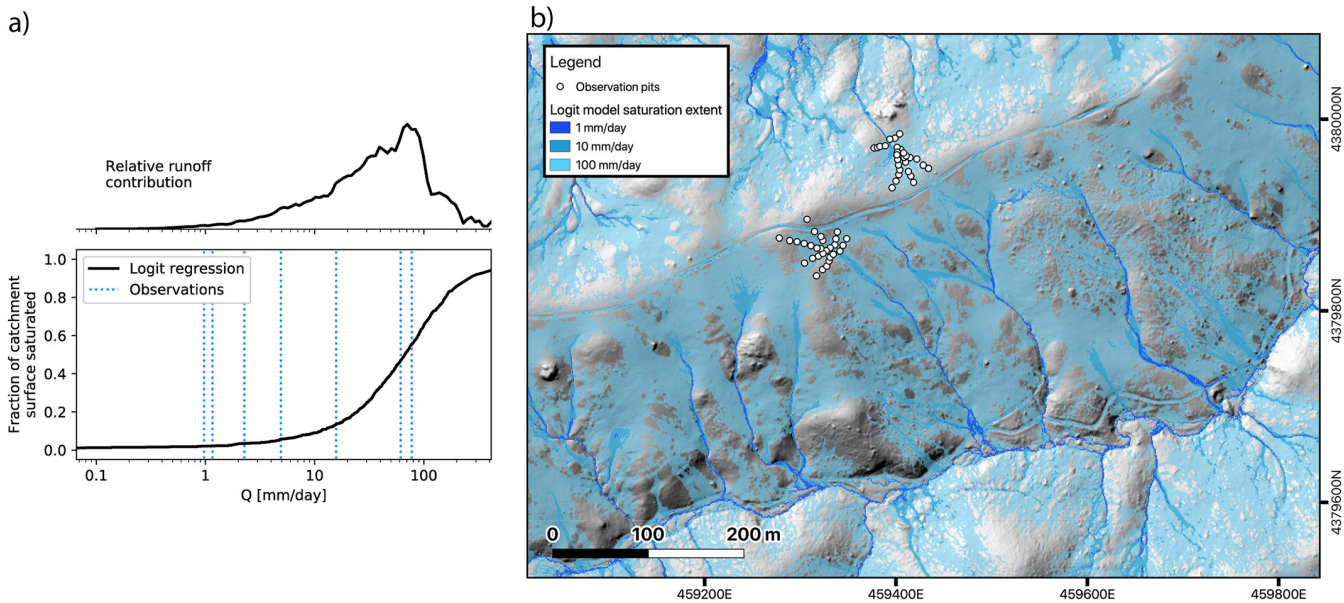

Figure 7. (a) Flow-weighted frequency (top) of instantaneous runoff magnitudes in the Dry Creek catchment. The 5th, 50th, and 95th percentiles flow-weighted frequencies are 20, 90, 320 mm/day, respectively. The median frequency-magnitude flow value coincides with times when a significant (approximately 60% by area) portion of the catchment is saturated, as predicted using the logistic regression model. (b) Saturation extent at different instantaneous streamflow rates. White points show where saturated/not saturated observations were made in field surveys across a range of instantaneous streamflow values. A logistic regression model was fitted using these observations, predicting saturated state at each point in the catchment as a function of log-transformed discharge and topographic wetness index. Blue transparencies over hillshade highlight saturation spatial extent at three discrete streamflow values. Uncolored areas are predicted to not be saturated at an instantaneous streamflow rate of 100 mm/day.

3.2. Isotope Dynamics

Isotopic composition of 267 precipitation samples, 460 streamflow samples, and 46 groundwater samples is shown for the full range of flow percentiles in Figure 8d. Streamflow isotopic compositions are markedly damped compared to precipitation, as demonstrated by the larger spread of precipitation isotopes (blue) than streamflow isotopes (red) in the time series and dual isotope plots of Figure 8. The sensitivity of stream water isotopes to precipitation inputs over shorter timescale is shown in Figure 8. Individual samples of stream water isotopic composition tend to follow a highly damped pattern shifting with the long-term mean, with some larger

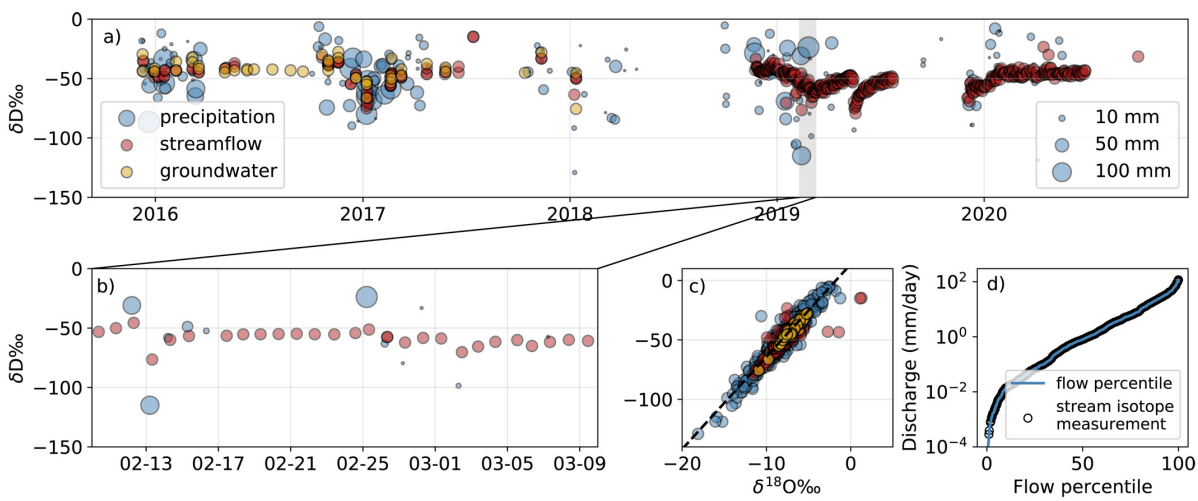

Figure 8. (a) Time series of 5 years of daily precipitation sampling, 3 years of episodic, and 2 years of daily streamflow sampling, and episodic groundwater sampling with a zoomed-in view for 1 month in 2019 (b). In (a, b), precipitation isotope markers are scaled by the volume of daily precipitation when the sample was taken. Panel (c) shows dual isotope space for all measurements, and (d) marks the time-weighted flow percentiles at which runoff was sampled.

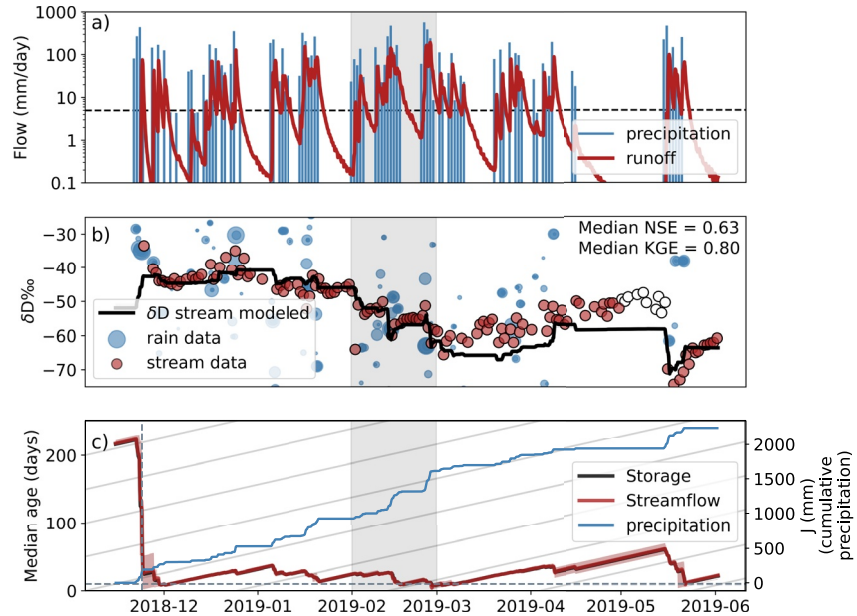

Figure 9. (a) Daily precipitation and instantaneous runoff throughout the wet season 2018–2019. Horizontal dashed black line marks the 5 mm flow threshold above which excess flow is assumed to be SOF. (b) Confidence bars on SAS model predictions (black line) are smaller than the width of the line. The size of plot markers for rainfall data (blue) are scaled by the volume of precipitation, and some rainfall falls outside the bounds of the plot. Full rainfall data are visible in Figure 8. Data shown in white circles are excluded from calibration of the SAS model due to in-channel evaporative enrichment (streamflow <0.05 mm/day). Marked median NSE and KGE are the median values among the top 95th percentile of parameter sets. (c) Shading around median ages indicates 25th–75th percentile of the tope 5th percentile of ensemble simulations, and blue line is cumulative precipitation. Storage and streamflow curves lie nearly on top of one another. Vertical dashed line marks cumulative precipitation of 150 mm, and horizontal dashed line marks a median age of 10 days. Shaded vertical bar indicates the timeframe shown in Figure 11.

excursions in the direction of individual rainfall inputs. In general, the relationship between precipitation and streamflow isotopic composition can be highly variable on a storm-to-storm basis. In the zoomed-in view in panel b, streamflow isotopic composition can change little with a large rainfall input (first and last large precipitation events) or be displaced significantly (as in the case of the large negative event or even the very small negative events in February and March). There is no repeated annual temporal trend in precipitation isotopic composition, unlike the characteristic sinusoidal signature of many continental climates (e.g., Allen et al., 2018, 2019; DeWalle et al., 1997). Instead, we observed a large degree of intraseasonal scatter in isotopic inputs.

At low discharge at the end of the wet season, streamflow samples show evidence of evaporative enrichment, likely due to evaporation of water in the stream channel during occasional long gaps in rain coupled with high atmospheric temperatures. Since evaporative enrichment is not accounted for in the SAS model, we excluded such samples from the SAS fitting. We identified a flow threshold of 0.05 mm/day, above which nearly all streamflow isotopic data fell on the meteoric water line (volume-weighted linear relationship between δD and δO in precipitation, Kendall & Caldwell, 1998). At flows below 0.05 mm/day, some streamflow samples fell on a line with a slope shallower than the local meteoric water line (Text S8 in Supporting Information S1). While not all flows below 0.05 mm/day show an evaporative enrichment signal, this threshold provides a conservative means of excluding evaporatively enriched samples from calibration. We compared our runoff threshold to a more standard method for identifying evaporative enrichment (lc-excess, Landwehr & Coplen, 2006). Our runoff threshold identifies 60% of the same measurements as the lc-excess method using a threshold of −4. The differences between these two methods should not impact results of the SAS model parameterization.

3.3. StorAge Selection Modeling

Figure 9 shows SAS modeling results for water year 2019. Results are similar for water year 2020, included in Figure S6 in Supporting Information S1. Among the top 95th percentile of parameter sets, median NSE and KGE

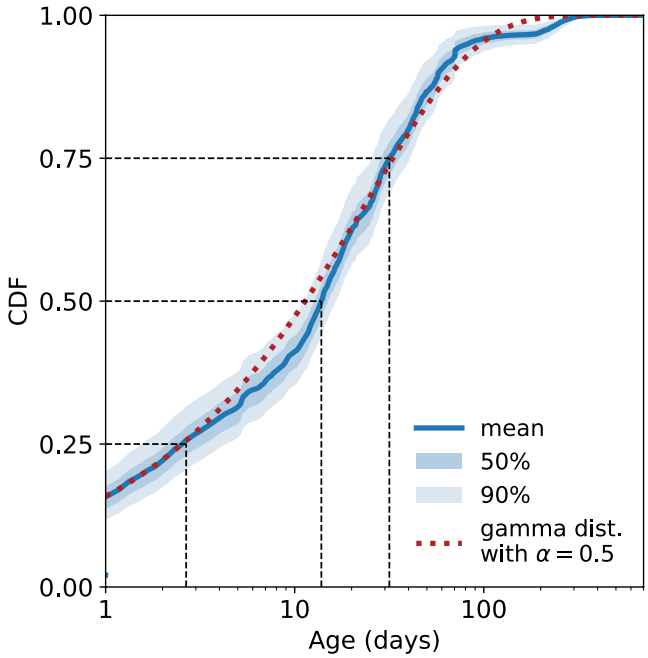

Figure 10. Ensemble mean of flow-weighted average cumulative age distribution function for Dry Creek. Shaded regions show the 25th–75th percentiles (50%) and the 5th-95th percentiles (90%) respectively. 25th percentile, median, and 75th percentile of streamflow age are 3 days, 14 days, and 32 days, respectively.

are 0.62 and 0.82, respectively. The range of NSE and KGE values among the top 95th percentile are 0.42–0.62 (NSE) and 0.82–0.83 (KGE). More details on model parameterization can be found in the Supporting Information S1. As shown in Figure 9b, the SAS model captures the moving average of streamflow isotope data, which shifts in time in response to precipitation inputs (Figure 9a); the model fails to capture the large negative daily excursions January and February and some small positive excursions in December and March. The unexplained large daily excursions suggest that higher temporal resolution in sampling could be beneficial. There is also a period of underestimated streamflow concentration in March-April of 2019, which may be due to a limitation in how the SAS model is applied on timescales shorter than the sampling period. While the SAS model has six parameters, results are really only sensitive to two of these parameters (Supporting Information S1), so additional flexibility in the model structure may be required to capture stream behavior in drier periods. In other words, only two parameters were well-constrained by the data (initial storage S_0 and the maximum value of k_Q). In other studies, S_0 was generally not well-constrained (e.g., Benettin et al., 2017), whereas the calibrated value matches our independent estimates of storage capacity (200 mm), suggesting that a smaller storage may be easier to constrain in the SAS modeling framework. We note also that the SAS model parameterized a small dynamic subsurface storage but still reproduced the highly damped streamflow isotope time series. White points, denoting when streamflow is <0.05 mm/day, were excluded from calibration and show an upward trend away from the model, consistent with significant evaporative enrichment (see Text S3 in Supporting Information S1).

At the end of the dry season, the median ages of water in storage modeled using SAS functions (Figure 9c) are slightly larger than the length of the dry season (5–6 months). Shortly after the onset of the wet season, median streamflow age declines rapidly with high confidence (narrow shaded band) after a short period of rainfall. This timeframe should be related to the time it takes to fill up approximately half of the catchment's dynamic storage capacity (although not identical since streamflow and ET draw preferentially from younger storage, delaying the drop). Indeed, the sharp decrease in median storage age within the confidence interval occurs at around 150 mm of cumulative precipitation, about three fourths of the estimated 200 mm dynamic storage capacity of the landscape (Dralle et al., 2018; Hahm, Rempe, et al., 2019). For nearly the whole wet season, median storage age is larger than 10 days (above the horizontal dashed line in Figure 9c). Results using mean age are essentially the same (see Supporting Information S1 and code).

Median ages of streamflow and storage modeled using SAS functions (Figure 9c) track one another closely throughout the wet season, falling on top of one another with overlapping confidence intervals, as is supported by SAS behavior close to random sampling under the most prevalent flow conditions (Figure S7 in Supporting Information S1). Storage age appears young since the storage modeled by the SAS function is only the dynamic portion of storage during the study period. Older storage may exist, but it accounts for only a small portion of dynamic storage so has essentially no impact on median ages.

Throughout the study period, the mean age distribution that results from the parameterized SAS function indicates that essentially all streamflow is younger than 1 year (Figure 10), the majority of water (~75%) is younger than 1 month, and about 15% of streamflow is younger than 1 day. More than 90% of streamflow is typically modeled to be younger than 4 months. This finding highlights that the vast majority of streamflow is fairly young, deriving from the current water year (i.e., the current wet season), and little long-term storage is included in catchment discharge.

3.4. Overland Flow Is Primarily Pre-Event Water

A summary of streamflow contributions from different runoff sources and water of different ages estimated via SAS modeling is shown in Table 2 and, for a representative month in 2019, in Figure 11. Only 1 month is

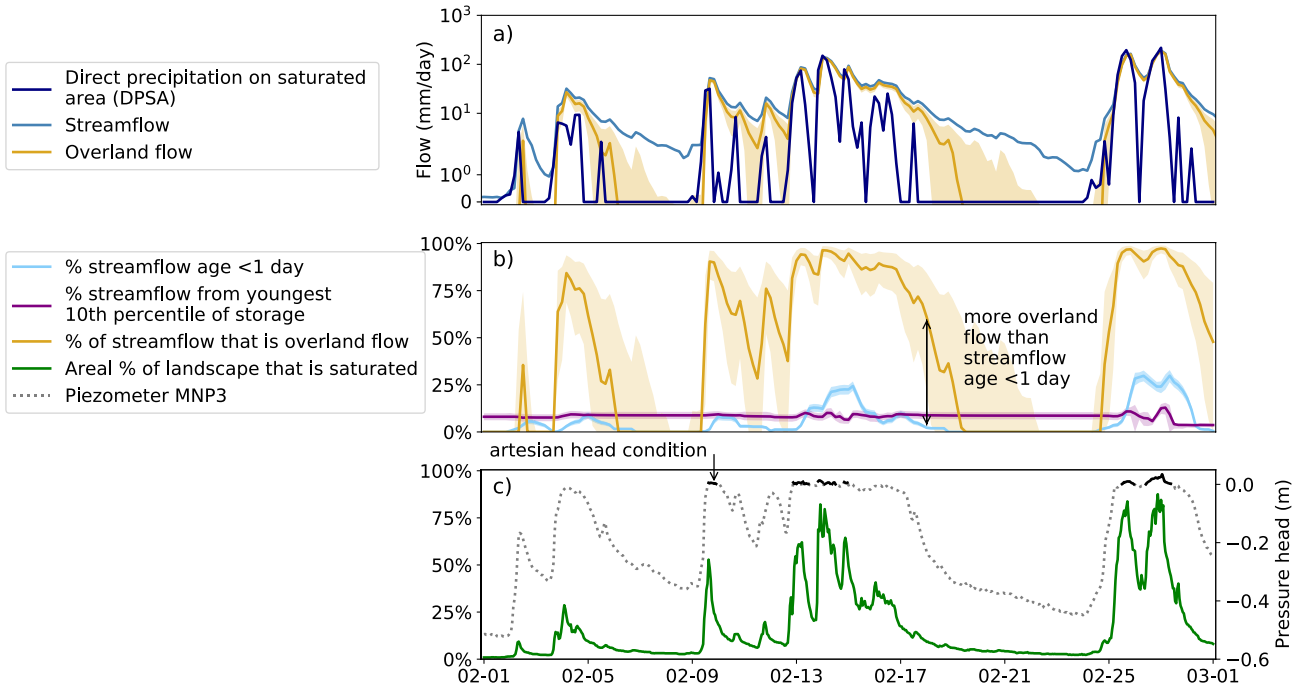

Figure 11. (a) Streamflow, estimated overland flow (streamflow above threshold instantaneous rate), and direct precipitation on saturated area (DPSA) for one representative month in 2019. See Sections 2.5 and 2.6 for descriptions of how DPSA and overland flow were calculated. Panel (b) compares the portion of streamflow derived from overland flow to streamflow water from the youngest tenth percentile of streamflow or water of age <1 day (c) Piezometer data and areal extents of saturation. Solid portions of piezometer data mark artesian head conditions. See Section 2.5 for a description of how saturation extent was calculated. Shaded intervals in (a, b) denote the 25th–75th percentiles of ensemble simulations except for overland flow. Shaded intervals for overland flow show a range of threshold streamflow values (2–10 mm/day; solid line best estimate of 5 mm/day) for initiation of overland flow throughout the catchment outside of the channel network.

shown for legibility, but all winter months in the study period show the same patterns. Using 5 mm/day (likely range of 2–10 mm/day) as the capacity for subsurface flow based on the saturation extent mapping analysis (see Figure 7b), we calculated overland flow as the difference between instantaneous streamflow and a catchment runoff rate of 5 mm/day (Figure 11a). In this analysis, all of this overland flow is considered to be saturation overland flow, as we have not observed any evidence for Horton overland flow at the site. Overland flow constitutes the majority of streamflow, nearly always accounting for more than 50% of streamflow during rainy periods and frequently accounting for more than 90% of flow during large storm events (Figure 11b); in general, overland flow accounts for 62–78% of annual streamflow (Table 2). This result is consistent with sustained high groundwater levels during storms (e.g., Figure 5b) and the prediction that 80% of the landscape is saturated in large storms (Figure 7a).

Figure 11b compares the fraction of streamflow from overland flow to two definitions of new water in streamflow calculated from the 95th percentile of parameter sets for the SAS model: (i) water <1 day old and (ii) water from the youngest tenth percentile of storage. Both of these estimates can be obtained as time series directly from the SAS model output by recording explicitly the fraction of streamflow at each timestep drawn from either definition of new water. Based on SAS modeling, water from the youngest tenth percentile of storage is consistently about 11% of streamflow, and only about 10% of streamflow is younger than 1 day on an annual basis (Table 2). Since the SAS model parameterizes the relationship between time series of precipitation isotopes and streamflow isotopes, these model results are driven by the highly damped nature of the streamflow time series compared to the precipitation time series.

Only 6–15% of annual streamflow is younger than 1 day, but 62–78% of streamflow derives from overland flow (Table 2). While errors in SAS performance (see Figure 9b) may result in a small under-prediction of new in streamflow, the difference between young water and overland flow volumes is too large to be a product of model error. Conservative estimates suggest that surface flow paths from the more distal portion of the watershed would reach the outlet within a day. We can approximate the travel paths as consisting of three distinct elements: sheet runoff on the ≈40 m long hillslope (e.g., Figure 1e), focused runoff down hollows and tributary channels

Table 2
Annual Streamflow Statistics by Water Year

Fraction of streamflow that derives from…	WY 2017	WY 2018	WY 2019	WY 2020
Overland flow	78%	70%	75%	62%
Water age <1 day	15%	9%	14%	6%
Water from youngest 10th percentile of storage	11%	11%	11%	11%
Direct precipitation on saturated area	40%	28%	37%	21%

(~500 m, e.g., Figure 1d), and travel down the mainstem Dry Creek (~4,000 m). Shallow sheet runoff is likely slow (on the order of 0.1 m/min), while in the hollows and channels velocities can exceed 5 m/min, and in the mainstem channel velocities exceed 10 m/min. These very conservative estimates would lead to the more distal part of the overland region reaching the outlet in about 15 hr. Hence, it is likely that overland flow across this landscape, if it remained on the surface and traveled to the outlet, would do so in less than a day.

Thus, the finding of significantly more overland flow than water younger than 1 day indicates that a large portion of overland flow must travel through the subsurface to reach the stream. Since all water following a singularly surface flow pathway would reach the outlet in less than 1 day, it is possible to set a limit on pre-event water in overland flow by comparing the fraction of streamflow younger than 1 day (light blue line in Figure 11b) to the fraction of streamflow derived from overland flow (gold line in Figure 11b). The difference between these two curves gives a lower bound on the pre-event water in overland flow, as marked in Figure 12. In Figure 12, we assumed that (at most) all water age <1 day arrived in the stream by overland flow. Then, given the difference in water volumes, at least 82% of overland flow in must be older than 1 day in water years 2019–2020. This finding is not unique to these years; throughout the study period, 81–90% of overland flow must be older than 1 day throughout each water year.

Further evidence for the importance of return flow to saturation overland flow comes from estimates of DPSA, calculated as the product of rainfall intensity and the percent saturated area (Figure 11a). The difference between this DPSA estimate and the overland flow curve places a different minimum bound on return flow contribution to streamflow since not all rain falling on saturated area necessarily contributes directly to runoff. Again, we

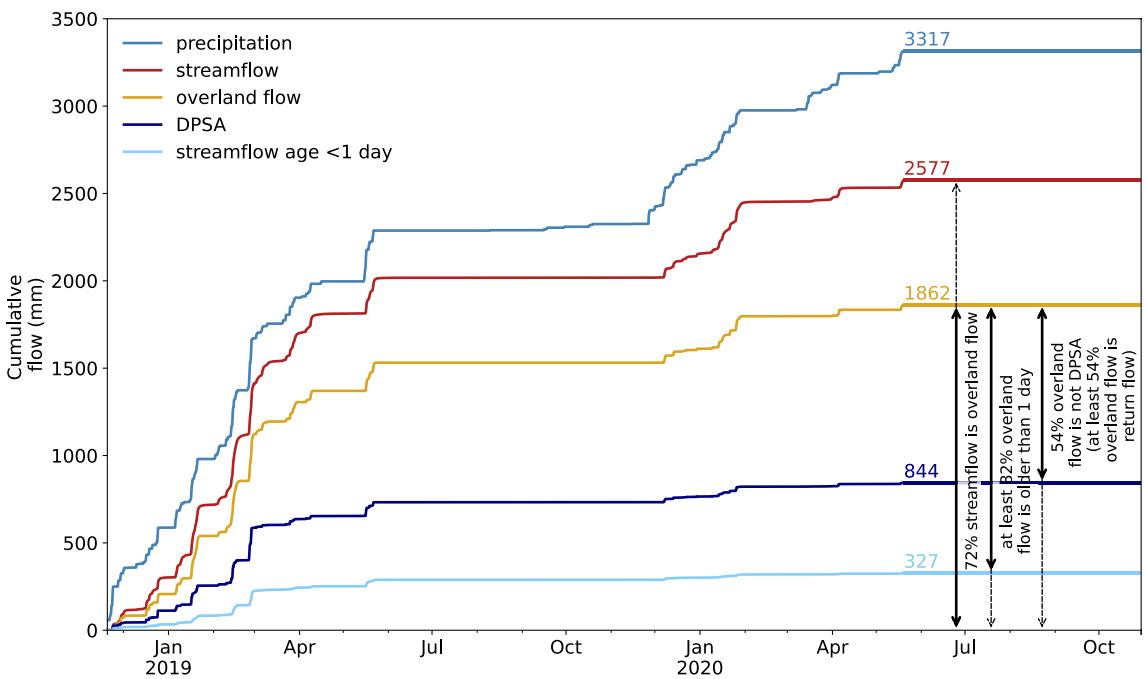

Figure 12. Cumulative amount of precipitation (light blue) compared to streamflow (red), overland flow using a threshold of 5 mm (gold), direct precipitation on saturated area, DPSA, (dark blue), and streamflow age <1 day (light blue). Numbers above each cumulative curve denote cumulative value for WY2019–2020.

see in Table 2 that at most 21–40% of streamflow could have been provided by DPSA, whereas overland flow accounts for 62–78% of streamflow on an annual basis. Thus, at least 49–66% of overland flow must be generated via return flow, providing further evidence that return flow plays an important role in saturation overland flow.

Overland flow accounts for the vast majority of streamflow, but water younger than 1 day and DPSA both account for relatively small fractions of annual runoff. These findings indicate that there must be substantial mixing between surface and subsurface water on the hillslope, which is also apparent in the damped isotopic signal of streamflow compared to rainfall (Figure 8).

4. Discussion

4.1. Pre-Event Water in Saturation Overland Flow

In spite of the thin critical zone and dominance of the saturation overland flow mechanism, flow that arrives in the stream at Dry Creek is on average days older than the storm that generated the streamflow. This indicates that: (a) precipitation is stored and overland flow must mix with older, pre-event water and (b) that water stored between events contributes substantially to saturation overland flow fluxes in events that follow. The storage and mixing have consequences for the conceptualization of runoff generation and water-rock interactions.

During periods of low flow between storm events (<approximately 2 mm/day), overland flow is not observed, and groundwater levels are below the ground surface across the borehole network. It is not until sufficient rains arrive to completely saturate the weathered bedrock and soil zone adjacent to the channel network that water tables intersect the ground surface and saturation overland flow is initiated. Further increases in streamflow are sustained by a continued rise of groundwater tables distal to the channel network and accompanying expansion of saturation extent (Figure 7b), leading to an increasing fraction of runoff that can be attributed to saturation overland flow, that is, variable source area (Dunne & Black, 1970b).

The apparent paradox of fast streamflow response paired with pre-event water has been observed for over 30 years (e.g., Buttle, 1994; Neal & Rosier, 1990; Sklash, 1990) and continues to be an active area of hydrologic inquiry (e.g., Cartwright & Morgenstern, 2018; Kirchner, 2003). Overland flow, for instance, results in a quick runoff response, and is often considered to represent new (event) water in hydrograph separation literature (e.g., Ogunkoya & Jenkins, 1993; Uhlenbrook et al., 2002). Our findings directly address the "old-water" paradox by demonstrating that, similar to the shallow subsurface stormflow observed by Kienzler and Naef (2008), saturation overland flow delivers pre-event water, and thus is older than the age of water delivered by the storm that generates streamflow. This is consistent with a recent particle tracking study that indicates that overland flow could primarily contain pre-event water while maintaining a streamflow signal that shows a predominance of young water catchment-wide (Wilusz et al., 2020). The behavior we observe at Dry Creek is similar to that of the Sleepers River watershed in Vermont, where saturation overland flow was originally documented. There, large extents (up to 50%) of the landscape can be saturated, saturation overland flow dominates runoff generation, and yet streamflow is nevertheless still largely older water (Shanley et al., 2015). Similarly, Eshleman et al. (1993), working in the Virginia Coastal Plain, found that saturation overland flow must consist primarily of return flow, based on the predominance of old-water in streamflow when saturation overland flow was the primary runoff generation mechanism.

Importantly, our results indicate that saturation overland flow and Horton or infiltration excess overland flow should have different signatures in the age distribution of streamflow since in Horton excess overland flow, the interaction with subsurface water pools is likely to be more limited (Horton, 1933, 1945). In the case of Horton overland flow, we would anticipate primarily surface flow paths and thus delivery of new, event water to streamflow, as has been found in locations where low surface hydraulic conductivity prevents infiltration (e.g., Ribolzi et al., 2007).

4.2. Do Seasonally Dry Catchments Discharge Younger Water at Wetter Catchment States?

Many catchments have a propensity to discharge younger water at wetter catchment states (the inverse storage effect, e.g., Benettin et al., 2017; Harman, 2015). This is in contrast to a well-mixed storage, where larger storage values make the output older. Preferential discharge of younger water at wetter catchment states has been directly observed in laboratory experiments (e.g., Kim et al., 2016) and inferred from particle tracking

(e.g., Pangle et al., 2017; Wilusz et al., 2020). This behavior may be more prevalent in some catchments than others based on particular climates or runoff generation mechanisms. Heidbüchel et al. (2012) found distinct differences in SAS behavior between a semiarid and a humid catchment. Most applications of SAS modeling have been in catchments with limited seasonality, so it is necessary to confirm whether seasonal catchments also tend to discharge younger water at wetter catchment states; recently, Rodriguez et al. (2018) found that the behavior holds in a catchment with a highly seasonal Mediterranean climate. In this study, based on parameterization results, the SAS function approximates random sampling behavior as the catchment state becomes drier (less SOF) and exhibits a strong preference for the youngest water in storage at the wettest state (more SOF; see Supporting Information S1 for details). However, over the course of the study period, the flow-weighted average value of the power exponent k is 0.99 (random sampling is $k = 1$), indicating that most streamflow in Dry Creek is sampled nearly randomly from available storage except during extremely wet periods. Thus, while there is evidence for greater discharge of young water at wetter catchment states at Dry Creek, streamflow predominantly reflects random sampling during the study period. For a time series of k over the study period, see Figure S7 in Supporting Information S1.

While Rodriguez et al. (2018) found in a Mediterranean climate that younger water was discharged at wetter catchment states, they found that this may not be the case during transitions between wet and dry seasons in the spring and fall. In our modeling, we allow the SAS function to vary through time according to wetness state, but the relationship between wetness state and SAS function remains constant throughout the study period. As a result, we are unable to determine whether a change in this relationship between wetness state and SAS function behavior occurs at our site. However, Figure 9a (streamflow time series in 2019) shows that the runoff goes down to about 0.1 mm/day numerous times over the wet season, indicating significant rapid shifts in catchment wetness throughout the season while the SAS model continues to perform well, missing few large concentration excursions. Parameterization on 2016–2019 water years also results in similarly good performance on the 2020 water year. There is, however, slightly higher absolute error in modeled concentrations during times of rapid state change versus continuously wet periods (Figure S7 in Supporting Information S1), and some excursions from the modeled isotopic concentrations correlate with transitions between wet and dry states. This suggests that there may be more older water discharged during transitions between wet and dry states in the Dry Creek catchment. While this effect was not included in our model, these transitions represent a very small portion of the study period so neglecting this effect should have a minimal impact on the results, particularly since our study focuses on SOF, and SOF does not occur during transitions between wet and dry states.

4.3. Assumptions and Limitations

Water age calculations assumed that the entire catchment met a water storage capacity quantified as a streamflow threshold; however, the storage capacity of the landscape is met dynamically through time so that some parts of the landscape may contribute overland flow before the full storage capacity of the subsurface is met. We do not have data to quantify the extent to which this effect may be important at Dry Creek, although results from a particle tracking study conducted by Wilusz et al. (2020) suggest that this effect is minimal. Wilusz et al. (2020) found that maximum groundwater discharge level during different parts of the hydrograph was a function of storage, above which flow derives from overland flow, interflow, or direct runoff (i.e., rain falling directly in the stream channel). Across different portions of the hydrograph, the threshold varied by only about a factor of 2. A constant flow threshold, as used in this study, should provide a reasonable estimate for the fraction of streamflow attributable to overland flow over timescales longer than a few hours. Differences in the time to reach storage capacity across the landscape at this temporal resolution should be negligible, and a difference of a factor of two is included in the shaded interval in Figure 11b.

In our analysis, we have assumed that we can scale our hillslope-scale observations (in locations underlain by mélange matrix) to the entire Dry Creek catchment. Lovill et al. (2018), Hahm et al. (2020), and Hahm, Rempe, et al. (2019) documented the presence of large sandstone blocks, which cover less than 15% of the catchment by area and behave hydrologically distinctly from the mélange matrix areas. In contrast to the mélange matrix, the sandstone blocks: (a) are deeply weathered; (b) have a thick vadose zone (>5 m), below which fluctuates a seasonal groundwater table; and (c) are observed to be the source of springs that persist into the mid-dry season. Because they are a relatively small portion of the landscape and because we are primarily interested in high-flow dynamics, we opted for the sake of simplicity to not separately model these features. The relatively high model performance (NSE = 0.62) provides some justification for this choice, but future work would benefit from

extended analysis of the sandstone blocks, which likely have an outsize contribution to streamflow at low flow states (Lovill et al., 2018).

5. Conclusion

In the Dry Creek catchment in the Northern California Coast Ranges, field observations and stream age modeling using StorAge Selection (SAS) functions reveal that saturation overland flow arriving in the channel is pre-event water. Field observations reveal that runoff dynamics are fast (response within a few hours of rainfall), with runoff coefficients as high as 0.9, and that saturation overland flow is the primary storm runoff mechanism. SAS modeling does not indicate a pronounced increase in young water fraction at wetter catchment states at Dry Creek except at extremely high flows. Although streamflow is modeled to be relatively young, the SAS model suggests that streamflow is still almost entirely older than 1 day at all times, meaning that streamflow is modeled to be older than event water. Since streamflow is primarily overland flow, the SAS modeling results imply that overland flow must contain a substantial portion of pre-event water. This finding is supported by field observations of exfiltrating head gradients, return flow through macropores, and extensive saturation days after storm events, which collectively point to a significant subsurface origin (i.e., return flow) for the saturation overland flow. Even in this extreme case of full catchment SOF, our analyses indicate that substantial mixing of overland flow with subsurface storage must occur to explain the observed streamflow ages.

Understanding the relationship between the age of streamflow and runoff generation mechanisms assists in understanding of how water quality may change over time, particularly under climate change. An increase in extreme precipitation with the same mean, as is expected with climate change in some locations, including California where our site is located (Swain et al., 2018), will lead to larger overland flow runoff events. This trend is likely to make overland flow more important in catchments where overland flow occurs. Increased precipitation volatility is also likely to result in increased relative variability in wetted channel extent (Lapides et al., 2021), which may apply to saturated area as well. Future studies might consider these interactions and their consequences for kinetic-rate controlled processes like chemical weathering.

Data Availability Statement

All data and code associated with the manuscript are available at https://www.hydroshare.org/resource/13244d-68f3e74452a8bbcb5d8860768c/ (Lapides et al., 2022). Code used in this study can also be accessed via Google Colab: https://colab.research.google.com/drive/1fB9BNEY7RzaGpqqnjo7gdeq79Bhqbjvb?usp=sharing (isotope and groundwater processing code), https://colab.research.google.com/drive/1EFI1GkU0DlgG56A-J17716UlxXc17W2Yd?usp=sharing (SAS modeling code), https://colab.research.google.com/drive/1VDtkjJG-jBOr0mXBq1--CLxVHmDLbGifZ?usp=sharing (logistic regression for saturation extent code), https://colab.research.google.com/drive/1FzbUSYS6OeKAOI02a35qZfktN72Ypzaz?usp=sharing (event runoff coefficient analysis), and https://colab.research.google.com/drive/1F4H-Mb-DfltsCp8mFvXDOceD7sJVhew5?usp=sharing (lag to peak analysis).

Acknowledgments
We gratefully acknowledge field access provided by Marilyn and Jerry Russell, and thank Renee Holleman for helping to collect precipitation and stream samples. Wenbo Yang, Todd Dawson, Collin Bode, Hunter Jamison, Sky Lovill, Colleen Murphy, and Sami Cargill contributed to fieldwork and laboratory analyses. Funding was provided by Simon Fraser University, a Natural Science Engineering Research Council of Canada Discovery Grant, the US National Science Foundation-supported Eel River Critical Zone Observatory (EAR 1331940), Oak Ridge Institute for Science and Education (ORISE), the University of California Natural Reserve System Mildred E. Mathias Graduate Student Research Grant, and the Carol Baird Fund for Graduate Field Science.

References

Abdul, A., & Gillham, R. (1984). Laboratory studies of the effects of the capillary fringe on streamflow generation. *Water Resources Research*, *20*(6), 691–698. https://doi.org/10.1029/WR020i006p00691

Allen, S. T., Jasechko, S., Berghuijs, W. R., Welker, J. M., Goldsmith, G. R., & Kirchner, J. W. (2019). Global sinusoidal seasonality in precipitation isotopes. *Hydrology and Earth System Sciences*, *23*(8), 3423–3436. https://doi.org/10.5194/hess-23-3423-2019

Allen, S. T., Kirchner, J. W., & Goldsmith, G. R. (2018). Predicting spatial patterns in precipitation isotope (δ2H and δ18O) seasonality using sinusoidal isoscapes. *Geophysical Research Letters*, *45*, 4859–4868. https://doi.org/10.1029/2018GL077458

Atwater, T., & Stock, J. (1998). Pacific-north America plate tectonics of the neogene southwestern United States: An update. *International Geology Review*, *40*(5), 375–402. https://doi.org/10.1080/00206819809465216

Baumhoff, M. A., & Merriam, C. H. (1958). *California Athabascan groups*. University of California Press.

Benettin, P., & Bertuzzo, E. (2018). tran-sas v1. 0: A numerical model to compute catchment-scale hydrologic transport using storage selection functions. *Geoscientific Model Development*, *11*, 1627–1639. https://doi.org/10.5194/gmd-11-1627-2018

Benettin, P., Soulsby, C., Birkel, C., Tetzlaff, D., Botter, G., & Rinaldo, A. (2017). Using SAS functions and high-resolution isotope data to unravel travel time distributions in headwater catchments. *Water Resources Research*, *53*, 1864–1878. https://doi.org/10.1002/2016WR020117

Beven, K. J., & Kirkby, M. J. (1979). A physically based, variable contributing area model of basin hydrology/un modèle à base physique de zone d'appel variable de l'hydrologie du bassin versant. *Hydrological Sciences Journal*, *24*(1), 43–69. https://doi.org/10.1080/02626667909491834

Blume, T., Zehe, E., & Bronstert, A. (2007). Rainfall—Runoff response, event-based runoff coefficients and hydrograph separation. *Hydrological Sciences Journal*, *52*(5), 843–862. https://doi.org/10.1623/hysj.52.5.843

Botter, G., Bertuzzo, E., & Rinaldo, A. (2011). Catchment residence and travel time distributions: The master equation. *Geophysical Research Letters*, *38*, L11403. https://doi.org/10.1029/2011GL047666

Buttle, J. (1994). Isotope hydrograph separations and rapid delivery of pre-event water from drainage basins. *Progress in Physical Geography*, *18*(1), 16–41. https://doi.org/10.1177/030913339401800102

Cartwright, I., & Morgenstern, U. (2018). Using tritium and other geochemical tracers to address the "old water paradox" in headwater catchments. *Journal of Hydrology*, *563*, 13–21. https://doi.org/10.1016/j.jhydrol.2018.05.060

Cloos, M. (1983). Comparative study of melange matrix and metashales from the Franciscan subduction complex with the basal great valley sequence, California. *The Journal of Geology*, *91*(3), 291–306. https://doi.org/10.1086/628772

DeWalle, D., Edwards, P., Swistock, B., Aravena, R., & Drimmie, R. (1997). Seasonal isotope hydrology of three appalachian forest catchments. *Hydrological Processes*, *11*(15), 1895–1906. https://doi.org/10.1002/(sici)1099-1085(199712)11:15<1895::AID-HYP538>3.0.CO;2-

Dietrich, W. (2015). *Laytonville, ca lidar 2015 airborne lidar survey*(distributed by OpenTopography). National Center for Airborne Laser Mapping (ncalm). https://doi.org/10.5069/G9WH2N2P

Dingman, S. L. (2015). *Physical hydrology*. Waveland Press.

Dralle, D. N., Hahm, W., Rempe, D. M., Karst, N. J., Thompson, S. E., & Dietrich, W. E. (2018). Quantification of the seasonal hillslope water storage that does not drive streamflow. *Hydrological Processes*, *32*(13), 1978–1992. https://doi.org/10.1002/hyp.11627

Dunne, T. (1978). Field studies of hillsope flow processes. In M. J. Kirkby (Ed.), *Hillslope hydrology*(pp. 227–293). Chichester, UK: Wiley.

Dunne, T., & Black, R. D. (1970a). An experimental investigation of runoff production in permeable soils. *Water Resources Research*, *6*(2), 478–490. https://doi.org/10.1029/WR006i002p00478

Dunne, T., & Black, R. D. (1970b). Partial area contributions to storm runoff in a small new England watershed. *Water Resources Research*, *6*(5), 1296–1311. https://doi.org/10.1029/WR006i005p01296

Elsenbeer, H., & Lack, A. (1996). Hydrometric and hydrochemical evidence for fast flowpaths at La Cuenca, Western Amazonia. *Journal of Hydrology*, *180*(1), 237–250. https://doi.org/10.1016/0022-1694(95)02889-7

Elsenbeer, H., West, A., & Bonell, M. (1994). Hydrologic pathways and stormflow hydrochemistry at South Creek, northeast Queensland. *Journal of Hydrology*, *162*(1), 1–21. https://doi.org/10.1016/0022-1694(94)90002-7

Eshleman, K. N., Pollard, J. S., & O'Brien, A. K. (1993). Determination of contributing areas for saturation overland flow from chemical hydrograph separations. *Water Resources Research*, *29*(10), 3577–3587. https://doi.org/10.1029/93WR01811

Foster, G. M. (1944). *A summary of Yuki culture* (Vol. 50). Berkeley, CA: University of California Press.

Freyberg, J. v., Studer, B., Rinderer, M., & Kirchner, J. W. (2018). Studying catchment storm response using event-and pre-event-water volumes as fractions of precipitation rather than discharge. *Hydrology and Earth System Sciences*, *22*(11), 5847–5865. https://doi.org/10.5194/hess-22-5847-2018

Godsey, S. E., Aas, W., Clair, T. A., De Wit, H. A., Fernandez, I. J., Kahl, J. S., et al. (2010). Generality of fractal 1/f scaling in catchment tracer time series, and its implications for catchment travel time distributions. *Hydrological Processes*, *24*(12), 1660–1671. https://doi.org/10.1002/hyp.7677

Group, P. C. (2013). PRISM climate data. Oregon State University. https://prism.oregonstate.edu

Haggerty, R., Wondzell, S. M., & Johnson, M. A. (2002). Power-law residence time distribution in the hyporheic zone of a 2nd-order mountain stream. *Geophysical Research Letters*, *29*(13), 18–21. https://doi.org/10.1029/2002GL014743

Hahm, W. J., Dietrich, W. E., & Dawson, T. E. (2018). Controls on the distribution and resilience of quercus garryana: Ecophysiological evidence of oak's water-limitation tolerance. *Ecosphere*, *9*(5), e02218. https://doi.org/10.1002/ecs2.2218

Hahm, W. J., Dralle, D., Lovill, S., Rose, J., Dawson, T., & Dietrich, W. (2017). Exploratory tree survey (2016—eel river critical zone observatory—Sagehorn—Central belt melange, Franciscan complex, northern California coast ranges, USA). *HydroShare*.

Hahm, W. J., Dralle, D., Rempe, D., Bryk, A., Thompson, S., Dawson, T., & Dietrich, W. (2019). Low subsurface water storage capacity relative to annual rainfall decouples mediterranean plant productivity and water use from rainfall variability. *Geophysical Research Letters*, *46*, 6544–6553. https://doi.org/10.1029/2019GL083294

Hahm, W. J., Dralle, D. N., Dawson, T. E., & Dietrich, W. E. (2020). Oak transpiration drawn from the weathered bedrock vadose zone in the summer dry season. *Water Resources Research*, *56*, e2020WR027419. https://doi.org/10.1029/2020WR027419

Hahm, W. J., Rempe, D. M., Dralle, D. N., Dawson, T. E., Lovill, S. M., Bryk, A. B., et al. (2019). Lithologically controlled subsurface critical zone thickness and water storage capacity determine regional plant community composition. *Water Resources Research*, *55*, 3028–3055. https://doi.org/10.1029/2018WR023760

Harman, C. J. (2015). Time-variable transit time distributions and transport: Theory and application to storage-dependent transport of chloride in a watershed. *Water Resources Research*, *51*, 1–30. https://doi.org/10.1002/2014WR015707

Harman, C. J., Evans, O., & Lu, F. (2019). *Mesas*. Retrieved from https://github.com/charman2/mesas

Heidbüchel, I., Troch, P. A., Lyon, S. W., & Weiler, M. (2012). The master transit time distribution of variable flow systems. *Water Resources Research*, *48*, W06520. https://doi.org/10.1029/2011WR011293

Hewlett, J. D., & Hibbert, A. R. (1967). Factors affecting the response of small watersheds to precipitation in humid areas. *Forest Hydrology*, *1*, 275–290.

Horton, R. E. (1933). The role of infiltration in the hydrologic cycle. *Eos, Transactions American Geophysical Union*, *14*(1), 446–460. https://doi.org/10.1029/TR014i001p00446

Horton, R. E. (1945). Erosional development of streams and their drainage basins; hydrophysical approach to quantitative morphology. *The Geological Society of America Bulletin*, *56*(3), 275–370. https://doi.org/10.1130/0016-7606(1945)56[275:EDOSAT]2.0.CO;2

Hrachowitz, M., Stockinger, M., Coenders-Gerrits, M., van der Ent, R., Bogena, H., Lücke, A., & Stumpp, C. (2021). Reduction of vegetation-accessible water storage capacity after deforestation affects catchment travel time distributions and increases young water fractions in a headwater catchment. *Hydrology and Earth System Sciences*, *25*(9), 4887–4915. https://doi.org/10.5194/hess-25-4887-2021

Jayko, A., Blake, M., McLaughlin, R., Ohlin, H., Ellen, S., & Kelsey, H. (1989). *Reconnaissance geologic map of the covelo 30-by 60-minute quadrangle, northern California* (Tech. Rep. No. MF-2001). US Government Printing Office.

Johnson, S. G. (1979). *The land-use history of the coast range preserve, Mendocino County, California* (Unpublished doctoral dissertation). San Francisco, CA: San Francisco State University.

Kelsey, H. M. (1978). Earthflows in Franciscan melange, van Duzen river basin, California. *Geology*, *6*(6), 361–364. https://doi.org/10.1130/0091-7613(1978)6<361:eifmvd>2.0.co;2

Kendall, C., & Caldwell, E. A. (1998). Fundamentals of isotope geochemistry. In *Isotope tracers in catchment hydrology* (pp. 51–86). Elsevier. https://doi.org/10.1016/b978-0-444-81546-0.50009-4

Kidron, G. J. (2021). Comparing overland flow processes between semiarid and humid regions: Does saturation overland flow take place in semiarid regions? *Journal of Hydrology*, *593*, 125624. https://doi.org/10.1016/j.jhydrol.2020.125624

Kienzler, P. M., & Naef, F. (2008). Subsurface storm flow formation at different hillslopes and implications for the 'old water paradox. *Hydrological Processes: International Journal*, *22*(1), 104–116. https://doi.org/10.1002/hyp.6687

Kim, M., Pangle, L. A., Cardoso, C., Lora, M., Volkmann, T. H., Wang, Y., et al. (2016). Transit time distributions and storages election functions in a sloping soil lysimeter with time-varying flow paths: Direct observation of internal and external transport variability. *Water Resources Research*, *52*, 7105–7129. https://doi.org/10.1002/2016WR018620

Kirchner, J. W. (2003). A double paradox in catchment hydrology and geochemistry. *Hydrological Processes*, *17*(4), 871–874. https://doi.org/10.1002/hyp.5108

Kirchner, J. W., Feng, X., & Neal, C. (2000). Fractal stream chemistry and its implications for contaminant transport in catchments. *Nature*, *403*(6769), 524–527. https://doi.org/10.1038/35000537

Kirkby, M. (1988). Hillslope runoff processes and models. *Journal of Hydrology*, *100*(1–3), 315–339. https://doi.org/10.1016/0022-1694(88)90190-4

Knoben, W. J., Freer, J. E., & Woods, R. A. (2019). Inherent benchmark or not? Comparing Nash-Sutcliffe and Kling-Gupta efficiency scores. *Hydrology and Earth System Sciences*, *23*(10), 4323–4331. https://doi.org/10.5194/hess-23-4323-2019

Landwehr, J., & Coplen, T. (2006). Line-conditioned excess: A new method for characterizing stable hydrogen and oxygen isotope ratios in hydrologic systems. In *International conference on isotopes in environmental studies* (pp. 132–135). International Atomic Energy Agency.

Lapides, D. A., Hahm, W., Rempe, D. M., Dietrich, W. E., & Dralle, D. N. (2022). *Calculating streamwater age using storage selection functions at Dry Creek, CA*. HydroShare. Retrieved from https://www.hydroshare.org/resource/f2c9289de92a41f5b5ca0590bfbe4ad1/

Lapides, D. A., Leclerc, C. D., Moidu, H., Dralle, D. N., & Hahm, W. (2021). Variability of stream extents controlled by flow regime and network hydraulic scaling. *Hydrological Processes*, *35*, e14079. https://doi.org/10.1002/hyp.14079

Latron, J., Soler, M., Llorens, P., & Gallart, F. (2008). Spatial and temporal variability of the hydrological response in a small Mediterranean research catchment (Vallcebre, Eastern Pyrenees). *Hydrological Processes*, *22*(6), 775–787. https://doi.org/10.1002/hyp.6648

Li, L., Sullivan, P. L., Benettin, P., Cirpka, O. A., Bishop, K., Brantley, S. L., et al. (2020). Toward catchment hydro-biogeochemical theories. *Wiley Interdisciplinary Reviews*, *8*(1), e1495.

Litwin, D. G., Tucker, G. E., Barnhart, K. R., & Harman, C. J. (2020). GroundwaterDupuitPercolator: A Landlab component for groundwater flow. *Journal of Open Source Software*, *5*(46), 1935. https://doi.org/10.21105/joss.01935

Lock, J., Kelsey, H., Furlong, K., & Woolace, A. (2006). Late neogene and quaternary landscape evolution of the northern California coast ranges: Evidence for mendocino triple junction tectonics. *The Geological Society of America Bulletin*, *118*(9–10), 1232–1246. https://doi.org/10.1130/b25885.1

Lovill, S., Hahm, W., & Dietrich, W. (2018). Drainage from the critical zone: Lithologic controls on the persistence and spatial extent of wetted channels during the summer dry season. *Water Resources Research*, *54*, 5702–5726. https://doi.org/10.1029/2017WR021903

Małoszewski, P., & Zuber, A. (1982). Determining the turnover time of groundwater systems with the aid of environmental tracers: 1. Models and their applicability. *Journal of Hydrology*, *57*(3–4), 207–231.

McDonnell, J. J., Spence, C., Karran, D. J., Ilja van Meerveld, H., & Harman, C. (2021). Fill-and-spill: A process description of runoff generation at the scale of the beholder. *Water Resources Research*, *57*, e2020WR027514. https://doi.org/10.1029/2020WR027514

Nash, J. E., & Sutcliffe, J. V. (1970). River flow forecasting through conceptual models. Part I—A discussion of principles. *Journal of Hydrology*, *10*(3), 282–290. https://doi.org/10.1016/0022-1694(70)90255-6

Neal, C., & Rosier, P. T. (1990). Chemical studies of chloride and stable oxygen isotopes in two conifer afforested and moorland sites in the British uplands. *Journal of Hydrology*, *115*(1–4), 269–283. https://doi.org/10.1016/0022-1694(90)90209-g

Ogunkoya, O., & Jenkins, A. (1993). Analysis of storm hydrograph and flow pathways using a three-component hydrograph separation model. *Journal of Hydrology*, *142*(1–4), 71–88. https://doi.org/10.1016/0022-1694(93)90005-t

Oshun, J., Dietrich, W. E., Dawson, T. E., & Fung, I. (2016). Dynamic, structured heterogeneity of water isotopes inside hillslopes. *Water Resources Research*, *52*, 164–189. https://doi.org/10.1002/2015WR017485

Pangle, L. A., Kim, M., Cardoso, C., Lora, M., Meira Neto, A. A., Volkmann, T. H., et al. (2017). The mechanistic basis for storage-dependent age distributions of water discharged from an experimental hillslope. *Water Resources Research*, *53*, 2733–2754. https://doi.org/10.1002/2016WR019901

Putnam, S. M. (2018). *The influence of landscape structure on storage and streamflow generation in a piedmont catchment* (Unpublished doctoral dissertation). Baltimore, MD: Johns Hopkins University.

Ribolzi, O., Karambiri, H., Bariac, T., Benedetti, M., Caquineaux, S., Descloitres, M., & Aventurier, A. (2007). Mechanisms affecting stormflow generation and solute behaviour in a Sahelian headwater catchment. *Journal of Hydrology*, *337*(1–2), 104–116. https://doi.org/10.1016/j.jhydrol.2007.01.019

Rinderer, M., Kollegger, A., Fischer, B. M., Stähli, M., & Seibert, J. (2012). Sensing with boots and trousers—Qualitative field observations of shallow soil moisture patterns. *Hydrological Processes*, *26*(26), 4112–4120. https://doi.org/10.1002/hyp.9531

Rittiman, C., Jr., & Thorson, T. (2001). *Soil survey of Mendocino county. California, western part*. Mendocino County Resource conservation District.

Rodhe, A., Nyberg, L., & Bishop, K. (1996). Transit times for water in a small till catchment from a step shift in the oxygen 18 content of the water input. *Water Resources Research*, *32*(12), 3497–3511. https://doi.org/10.1029/95WR01806

Rodriguez, N. B., & Klaus, J. (2019). Catchment travel times from composite storage selection functions representing the superposition of streamflow generation processes. *Water Resources Research*, *55*, 9292–9314. https://doi.org/10.1029/2019WR024973

Rodriguez, N. B., McGuire, K. J., & Klaus, J. (2018). Time-varying storage–water age relationships in a catchment with a mediterranean climate. *Water Resources Research*, *54*, 3988–4008. https://doi.org/10.1029/2017WR021964

Rodriguez, N. B., Pfister, L., Zehe, E., & Klaus, J. (2021). A comparison of catchment travel times and storage deduced from deuterium and tritium tracers using storage selection functions. *Hydrology and Earth System Sciences*, *25*(1), 401–428. https://doi.org/10.5194/hess-25-401-2021

Shanley, J. B., Kendall, C., Smith, T. E., Wolock, D. M., & McDonnell, J. J. (2002). Controls on old and new water contributions to stream flow at some nested catchments in Vermont, USA. *Hydrological Processes*, *16*(3), 589–609. https://doi.org/10.1002/hyp.312

Shanley, J. B., Sebestyen, S. D., McDonnell, J. J., McGlynn, B. L., & Dunne, T. (2015). Water's Way at Sleepers River watershed—Revisiting flow generation in a post-glacial landscape, Vermont USA. *Hydrological Processes*, *29*(16), 3447–3459. https://doi.org/10.1002/hyp.10377

Sklash, M. (1990). Environmental isotope studies of storm and snowmelt runoff generation. In M. G. Anderson & T. P. Burt (Eds.), *Process studies in hillslope hydrology* (pp. 401–436). Chichester, UK: John Wiley and Sons.

Sklash, M. G., & Farvolden, R. N. (1979). The role of groundwater in storm runoff. *Journal of Hydrology*, *43*(1–4), 45–65. https://doi.org/10.1016/s0167-5648(09)70009-7

Smith, A., Tetzlaff, D., & Soulsby, C. (2018). On the use of storage selection functions to assess time-variant travel times in lakes. *Water Resources Research*, *54*, 5163–5185. https://doi.org/10.1029/2017WR021242

Stewart, O. C. (1943). *Notes on Pomo ethnogeography*. University of California Press.

Swain, D. L., Langenbrunner, B., Neelin, J. D., & Hall, A. (2018). Increasing precipitation volatility in twenty-first-century California. *Nature Climate Change*, *8*(5), 427–433. https://doi.org/10.1038/s41558-018-0140-y

Torres, M. A., & Baronas, J. J. (2021). Modulation of Riverine concentration-discharge relationships by changes in the Shape of the water transit time distribution. *Global Biogeochemical Cycles*, *35*, e2020GB006694. https://doi.org/10.1029/2020GB006694

Uhlenbrook, S., Frey, M., Leibundgut, C., & Maloszewski, P. (2002). Hydrograph separations in a mesoscale mountainous basin at event and seasonal timescales. *Water Resources Research*, *38*(6), 31. https://doi.org/10.1029/2001WR000938

Van der Velde, Y., De Rooij, G., Rozemeijer, J., Van Geer, F., & Broers, H. (2010). Nitrate response of a lowland catchment: On the relation between stream concentration and travel time distribution dynamics. *Water Resources Research*, *46*, W11534. https://doi.org/10.1029/2010WR009105

Van Der Velde, Y., Torfs, P., Van Der Zee, S., & Uijlenhoet, R. (2012). Quantifying catchment-scale mixing and its effect on time-varying travel time distributions. *Water Resources Research*, *48*, W06536. https://doi.org/10.1029/2011WR011310

Visser, A., Thaw, M., Deinhart, A., Bibby, R., Safeeq, M., Conklin, M., et al. (2019). Cosmogenic isotopes unravel the hydrochronology and water storage dynamics of the southern sierra critical zone. *Water Resources Research*, *55*, 1429–1450. https://doi.org/10.1029/2018WR023665

Wilson, C., & Dietrich, W. (1987). *The contribution of bedrock groundwater flow to storm runoff and high pore pressure development in hollows* (Vol. 165, pp. 49–59). IAHS-AISH Publication.

Wilusz, D., Harman, C., Ball, W., Maxwell, R., & Buda, A. (2020). Using particle tracking to understand flow paths, age distributions, and the paradoxical origins of the inverse storage effect in an experimental catchment. *Water Resources Research*, *56*, e2019WR025140. https://doi.org/10.1029/2019WR025140

References From the Supporting Information

Craig, H. (1961). Isotopic variations in meteoric waters. *Science*, *133*(3465), 1702–1703. https://doi.org/10.1126/science.133.3465.1702

Gallart, F., Valiente, M., Llorens, P., Cayuela, C., Sprenger, M., & Latron, J. (2020). Investigating young water fractions in a small mediterranean mountain catchment: Both precipitation forcing and sampling frequency matter. *Hydrological Processes*, *34*(17), 3618–3634. https://doi.org/10.1002/hyp.13806